Component Dynamics in Polyisoprene/Poly(4-*tert*-butylstyrene) Miscible Blends

Quan Chen,[†] Yumi Matsumiya,[†] Yuichi Masubuchi,[†] Hiroshi Watanabe,*[,†] and Tadashi Inoue[‡]

Institute for Chemical Research, Kyoto University, Uji, Kyoto 611-0011, Japan, and Department of Macromolecular Science, Faculty of Science, Osaka University, Toyonaka, Osaka 560-0043, Japan

Received June 14, 2008; Revised Manuscript Received September 9, 2008

ABSTRACT: Linear viscoelastic and dielectric behavior was examined for blends of *cis*-polyisoprene (PI-20; $M_{PI} = 19.9 \times 10^3$) and poly(4-*tert*-butylstyrene) (PtBS-16; $M_{PtBS} = 16.4 \times 10^3$) with the PtBS concentration of $w_{PtBS} = 30$ and 50 wt %. At temperatures examined, $T \leq 120$ °C, the PI/PtBS blends were in a statically homogeneous state. Since PI had the type-A dipole while PtBS did not, the dielectric loss of the blends measured at low angular frequencies ω ($<10^5$ s^{-1}) was attributed exclusively to the global motion of PI chains. At low T and/or high w_{PtBS}, the dielectric loss data of the PI chains did not obey the time−temperature superposition, despite the static homogeneity in the blends. Comparison of the viscoelastic and dielectric data indicated that in the blends PtBS relaxed more slowly than PI. Thus, PtBS possibly gave an effectively quenched, nonuniform frictional environment in the time scale of *the global relaxation of PI*, and changes of this frictional nonuniformity with T appeared to result in the failure of the time−temperature superposition for the PI relaxation. In contrast, the superposition held for the terminal viscoelastic data of the slow component, PtBS, possibly because the frictional nonuniformity in the time scale of PtBS relaxation was erased by the fast PI chains. Furthermore, WLF analysis of the viscoelastic data revealed that the PtBS relaxation was slower, by a factor of 16 (for $w_{PtBS} = 30$ wt %) and 5 (for $w_{PtBS} = 50$ wt %), in the blends than in an iso-frictional bulk state. This result suggested that bulky PtBS chains were subjected to motional constraint (not identical but somewhat similar to the entanglement in homopolymer systems) due to the flexible PI chains, despite the fact that M_{PtBS} was not large enough to allow the PtBS chains to be entangled by themselves even at $w_{PtBS} = 100$ wt % (in bulk state). This constraint for low-M PtBS chains was discussed in relation to the concept of packing length.

1. Introduction

It is well established that miscible polymer blends still have a heterogeneity in their component chain concentrations in the *segmental length scale* because of the chain connectivity (that results in the self-concentration[1] of the segments of respective chains) as well as the dynamic fluctuation over various length scales.[1−8] Moreover, the segmental motion of each component may be restricted by the motional barrier within the chain and this effect is not necessarily the same, in magnitude, for different components. As a result, the blend components encounter different dynamic environments to exhibit different temperature dependencies in their segmental relaxation rates. This type of dynamic heterogeneity often results in a broad glass transition (sometimes seen as two separate transitions), a broad distribution of the segmental relaxation modes, and the thermo-rheological complexity of this distribution.[1−8] These effects of the dynamic heterogeneity tend to be enhanced when the component chains have widely separated glass transition temperatures T_g.[9−11]

Experimentally, the dynamic heterogeneity can be most conveniently studied for model binary blends in which the two components have different contributions to measurable properties. The component dynamics in such blends can be resolved through analysis of the properties. For this purpose, blends of *cis*-polyisoprene (PI) and poly(vinyl ethylene) (PVE), having a lower critical solution temperature (LCST) but being in a homogeneous state in a wide range of T, have been frequently utilized as model systems.[2−4,12,13] PI has both of the type-A and type-B dipoles[14,15] parallel along and perpendicular to the chain backbone, respectively, while PVE has only type-B dipoles. Thus, the slow dielectric response of the PI/PVE blends exclusively reflects the global motion of PI over its end-to-end distance R_{PI}, while the fast dielectric process (the so-called α-process due to the type-B dipole) detects the segmental motion of both of PI and PVE chains. For the PI/PVE blends, experiments[3,4,12,13] revealed the failure of the time−temperature superposition for the segmental relaxation of the blend as a whole as well as the broad glass transition due to the dynamic heterogeneity. However, the superposition worked for the terminal relaxation of *each* component. For example, Urakawa and co-workers[12,13] demonstrated the superposability for the dielectrically detected *global* relaxation of PI (=fast component in their blends). Correspondingly, Haley and co-workers[16,17] and Pathak and co-workers[11] treated each component as a thermo-rheologically simple component (at least in long time scales) and combined the concept of "double reptation" and "self-concentration" in their attempts of describing the viscoelastic data of blends. In particular, Haley and co-workers[16,17] observed changes of terminal mode distribution with the blend composition attributable to the composition dependencies of the entanglement molecular weight and segmental friction, not to the dynamic heterogeneity.

However, the dynamic situation in homogeneous blends may be more complicated under the conditions that (1) the concentration C of the slow component chains is *not* much larger than their overlapping concentration C^*, (2) the average end-to-end distance R_{fast} of the fast component chain (=length scale for the global relaxation of this chain) is *not* much larger than R_{slow} of the slow component chain, and (3) the fast and slow components have widely separated glass transition temperatures T_g in respective bulk states (which naturally results in a difference of their effective T_g in the blend and the corresponding difference of their local friction coefficients). The same degree of overlapping with the slow component chains cannot

* To whom correspondence should be addressed hiroshi@scl.kyoto-u.ac.jp.
[†] Institute for Chemical Research, Kyoto University.
[‡] Department of Macromolecular Science, Faculty of Science, Osaka University.

10.1021/ma8013417 CCC: $40.75
Published on Web 10/25/2008

be simultaneously achieved for all of the fast component chains if the conditions (1) and (2) are satisfied, and this nonuniformity of overlapping can results in a frictional nonuniformity for the global relaxation of the fast chains if the condition (3) is further satisfied.[18] Then, among the fast chains, some would feel a higher friction during their global relaxation compared to the others. This frictional distribution changes with temperature to result in the thermo-rheological complexity of the *terminal* relaxation of the fast component chains as a whole.

In fact, we have observed this complexity for a LCST-type blend of *cis*-polyisoprene (PI-20; $M_{PI} = 19._9 \times 10^3$, $R_{PI} = 12$ nm, and $T_{g,bulk}^{PI} \cong -70$ °C) and poly(4-*tert* butyl styrene) (PtBS-70; $M_{PtBS} = 69._5 \times 10^3$, $R_{PtBS} = 16$ nm, and $T_{g,bulk}^{PtBS} \cong 150$ °C) with the PtBS concentration of $w_{PtBS} = 20$ wt %.[18] This blend was in a homogeneous state at $T \leq 70$ °C, as confirmed from scattering experiments.[18,19] PtBS had no type-A dipole and was dielectrically inert in its terminal regime, which enabled us to compare the dielectric and viscoelastic data of the blend to specify that PI-20 and PtBS-70 were the fast and slow components, respectively. These components satisfied the above conditions (1)-(3);[18] $C_{PtBS} = 0.19$ g cm^{-3} which was less than twice of C_{PtBS}^* (= 0.10 g cm^{-3}), $R_{PI} < R_{PtBS}$, and $T_{g,bulk}^{PtBS} \gg T_{g,bulk}^{PI}$. Correspondingly, the failure of the time−temperature superposition was dielectrically observed for the terminal relaxation of the fast component PI-20 at $T \leq 70$ °C,[18] despite the static homogeneity at those T. It should be also noted that the superposition held for the same PI-20 chains in a blend with a lower-M PtBS-16 ($M_{PtBS} = 16._4 \times 10^3$ and $R_{PtBS} = 7.7$ nm) at the same PtBS concentration, $w_{PtBS} = 20$ wt %, quite possibly because PI-20 was the *slow* component in this blend and the frictional heterogeneity due to PtBS-16 was smeared in the time scale of the terminal relaxation of PI-20.[20] (In relation to this point, we note that the PI/PVE blends examined by Urakawa et al.[12,13] contained PI as the fast component but did not satisfy the conditions (1) and (3): C_{PVE} was much larger than C_{PVE}^* for the high-M PVE in their blends and $T_{g,bulk}^{PVE}$ (≅0 °C) was not sufficiently higher than $T_{g,bulk}^{PI}$, which could have allowed PI in their blends to obey the time−temperature superposition in the terminal relaxation regime.)

As explained above, the studies for the PI-20/PtBS-70 and PI-20/PtBS-16 blends[18,20] revealed a new feature of the miscible blends, the effect of the slow component on the frictional nonuniformity for the global relaxation of the fast component. However, there remain several issues for further study. The conditions (1)−(3) explained above are satisfied in the PI-20/PtBS-16 blend with $w_{PtBS} = 20$ wt % but the time−temperature superposition held for PI-20 in this blend possibly because PI-20 was the slow component. We expect that the superposition fails even in the PI-20/PtBS-16 blend if we increase w_{PtBS} to enhance a difference of effective T_g of PI-20 and PtBS-16 therein and force PI-20 to behave as the fast component. In addition, the PtBS-70 chains were barely entangled in its bulk state (because its M was less than twice of the bulk entanglement molecular weight,[21] $M_{e,bulk}^{PtBS}$ $M_{e,bulk}^{PtBS} = 37._6 \times 10^3$) but they appeared to be motionally constrained by (or, *entangled* with, in some sense) PI-20 chains in the PI-20/PtBS-70 blend.[18] We expect a similar motional constraint also for lower-M PtBS-16 chains in the PI-20/PtBS-16 blends with large w_{PtBS}.

Thus, we examined the linear viscoelastic and dielectric behavior of PI-20/PtBS-16 blends with $w_{PtBS} > 20$ wt % to examine these expectations. The failure of the time−temperature superposition was indeed observed for the PI-20 chains in the blends with $w_{PtBS} = 30$ and 50 wt % (where PI-20 behaved as the fast component). Furthermore, the PtBS-16 relaxation in these blends was slower than that in the *iso*-frictional bulk state, suggesting the motional constraint for the PtBS-16 chains due to the coexisting PI chains. This paper presents details of these results and discusses them on the basis of the concepts of Williams−Landel−Ferry (WLF)-type local friction[22] and packing length.[21,23,24]

Table 1. Characteristics of Samples

code	$10^{-3}M_w$	M_w/M_n	R^b/nm
PI-20[a]	$19._9$	1.10	12
PtBS-16	$16._4$	1.02	7.7

[a] Supplied from Kuraray Co. The microstructure was 1,4-*cis*:1,4-*trans*:3,4 = 79:14:7. [b] Root-mean-square end-to-end distance.

2. Experimental Section

2.1. Material. An atactic poly(4-*tert*-butyl styrene) sample (PtBS-16) anionically synthesized with *s*-butyllithium (initiator) in benzene[20] and a commercially available high-*cis* polyisoprene sample (PI-20; supplied from Kuraray Co.) were used. The microstructure of PI-20, determined from ^{1}H NMR, was 1,4-*cis*:1,4-*trans*:3,4 = 79:14:7. Table 1 summarizes the characteristics of the samples. The sample code numbers refer to $10^{-3}M_w$.

PI-20/PtBS-16 blends with the PtBS-16 concentration of $w_{PtBS} = 30$ and 50 wt % were subjected to viscoelastic, dielectric, and calorimetry measurements explained later. (The blend with $w_{PtBS} = 20$ wt % was examined in the previous study.[20]) The blends were prepared according to the method by Yurekli and Krishnamoorti:[19] Prescribed masses of PI-20 and PtBS-16 were first dissolved in tetrahydrofuran (THF) at a total concentration of 10 wt % and then drop-wisely precipitated into an excess methanol/acetone 8/2 mixture vigorously stirred by a magnetic bar. The blends were recovered *via* decantation, thoroughly dried in vacuum (first at room temperature and then at 85 °C), and utilized for the measurements. The blends thus obtained were transparent, which was in accordance with the phase behavior explained below.

PtBS and PI are known to exhibit the lower critical solution temperature (LCST)-type phase behavior.[19] However, the phase separation temperature T_c was inaccessibly high for PtBS and PI of $M \leq 10^5$. For example, scattering data suggested that blends of PI-20 ($M = 19._9 \times 10^3$) and PtBS-70 ($M_{PtBS} = 69._5 \times 10^3$) had $T_c \cong 250$ °C.[25] The blends of PI-20 with the lower-M PtBS-16 examined in this study should have had an even higher T_c and were in the statically homogeneous state at the temperatures examined ($T \leq 120$ °C).

2.2. Measurements. ^{1}H-MMR measurement was conducted to determine the microstructure of the PI-20 sample (dissolved in deuterated chloroform). A Varian MERCURYplus AS400 spectrometer was operated at a static magnetic field of 9.4 T and the resonance frequency of 400.0 MHz.

For the PI-20/PtBS-16 blends with $w_{PtBS} = 30$ and 50 wt %, linear viscoelastic measurements were conducted with a laboratory rheometer (ARES, Rheometrics) at temperatures $T \leq 120$ °C. A parallel-plate fixture of a diameter = 8 mm was utilized. The oscillatory strain amplitude was kept small ($\gamma_0 = 0.05$) to ensure the linearity of the storage and loss moduli G' and G'' measured as functions of the angular frequencies ω/s^{-1} in a range between 10^{-2} and 10^2.

Dielectric measurements were also conducted for those blends in the same temperature range, $T \leq 120$ °C. The blends were charged in a dielectric cell composed of parallel electrodes and a guard electrode, and the measurements were conducted with an impedance analyzer/dielectric interface system (1260 and 1296, Solartron) and a capacitance bridge (1615A, QuadTech). The dielectric loss ϵ'' was measured as a function of frequencies f ($<10^6$ Hz), and the ϵ'' data were summarized as plots against the angular frequency ω/s^{-1} ($= 2\pi f$). The dielectric relaxation attributed to the global motion of PI-20 in the blends was completed at fairly high ω where the direct current (dc) conduction had negligibly contributed to the ϵ'' data. Thus, this paper utilizes only *raw* ϵ'' data without any correction for the dc contribution.

Differential scanning calorimetry (DSC) measurements were conducted for the PI-20/PtBS-16 blends ($w_{PtBS} = 30$ and 50 wt %) as well as for bulk PI-20 and PtBS-16 samples with a laboratory

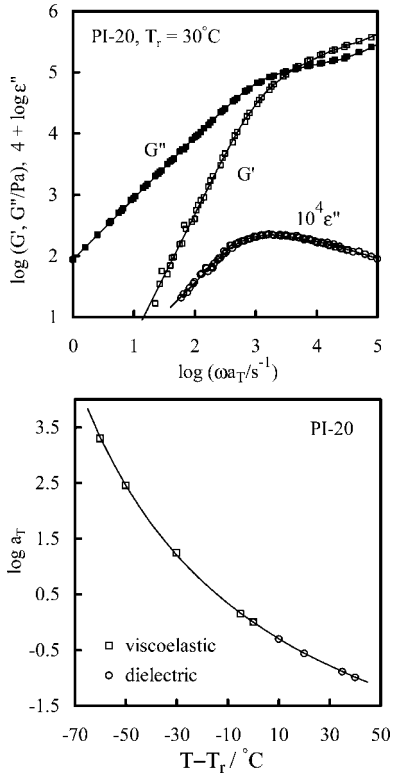

Figure 1. Top panel: Frequency dependence of storage and loss moduli, G' and G'', and dielectric loss, ϵ'', obtained for bulk PI-20 sample. All data are reduced at $T_{r,bulk} = 30$ °C. Bottom panel: Shift factors a_T obtained for the viscoelastic G^* data (squares) and dielectric ϵ'' data (circles). The solid curve indicates WLF eq 1. Redrawn, with permission, from ref 18.

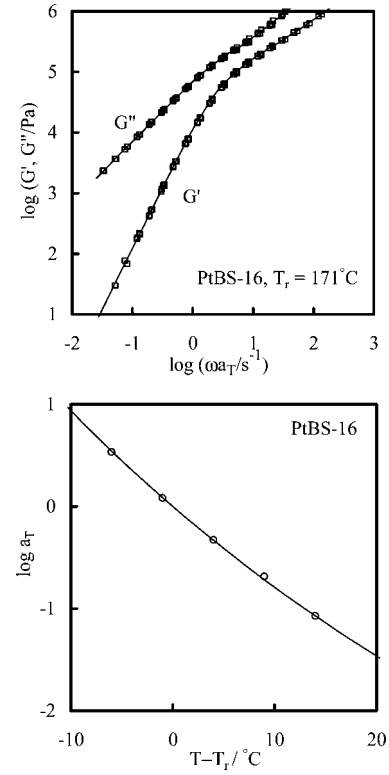

Figure 2. Top panel: Frequency dependence of storage and loss moduli, G' and G'', obtained for bulk PtBS-16 sample. The data are reduced at $T_{r,bulk} = 171$ °C. Bottom panel: Shift factor a_T obtained for the G^* data. The solid curve indicates WLF eq 2. Redrawn, with permission, from ref 20.

calorimeter (DSC2910; TA Instruments). The DSC traces were recorded for respective specimens (~10 mg) at a heating rate of 20 °C/min in a range of T between −100 and +200 °C.

3. Results and Discussion

3.1. Dynamic Behavior of Bulk Components. The dynamic behavior of the bulk PI-20 and PtBS-16 components was reported previously.[18,20] However, for convenience of later discussion for the PI-20/PtBS-16 blends, the angular frequency (ω) dependencies of their storage and loss moduli, $G'(\omega)$ and $G''(\omega)$, and their dielectric loss multiplied by a factor of 10^4, $10^4\epsilon''(\omega)$, are shown in the top panels of Figures 1 and 2. The time−temperature superposition held for those data, and respective shift factors a_T are shown in the bottom panels. The reference temperatures are $T_r = 30$ and 171 °C for bulk PI-20 and PtBS-16, respectively.

Since PI chains have the type-A dipoles parallel along the chain backbone, their global motion (large scale motion over the end-to-end distance) results in both of the terminal viscoelastic and dielectric relaxation processes characterized by power-law relationships, $G' \propto \omega^2$, $G'' \propto \omega$, and $\epsilon'' \propto \omega$. Correspondingly, these terminal processes of PI-20 emerge in the same range of ω as seen in the top panel of Figure 1, and the viscoelastic and dielectric shift factors excellently agree with each other; cf. bottom panel. These shift factors are well described by the WLF equation shown with the solid curve in the bottom panel[18]

$$\log a_T = -\frac{4.425(T - T_r)}{140.0 + T - T_r} \tag{1}$$

with $T_r = 30$ °C for bulk PI-20. Equation 1 is later utilized as a reference in the WLF analysis of the dielectric data of PI-20/PtBS-16 blends.

The PtBS-16 chains have no type-A dipole and thus their global motion just results in the terminal viscoelastic relaxation not associated with the dielectric relaxation; cf. top panel of Figure 2. (PtBS-16 has type-B dipole and its segmental motion activates the dielectric relaxation, but this relaxation emerges at high ω not covered in Figure 2.[20]) The viscoelastic shift factor of PtBS-16 is described by the WLF equation shown with the solid curve in the bottom panel: [20]

$$\log a_T = -\frac{10.0(T - T_r)}{116.5 + T - T_r} \tag{2}$$

with $T_r = 171$ °C for bulk PtBS-16. Equation 2 is later utilized as a reference in the WLF analysis of the viscoelastic data of PtBS-16 blended with PI-20.

Here, a comment needs to be made for the entanglement in bulk PI-20 and PtBS-16 systems. The entanglement molecular weight defined within the classical rubber elasticity theory, $M_e = \rho RT/G_N$ (ρ = density, R = gas constant, T = absolute temperature, and G_N = plateau modulus), is $M_{e,bulk}^{PI} = 5.0 \times 10^3$ and $M_{e,bulk}^{PtBS} = 37.6 \times 10^3$ for bulk PI[21] and bulk PtBS,[21] respectively. Thus, PI-20 chains ($M_{PI} = 19.9 \times 10^3 \cong 4M_{e,bulk}^{PI}$) are moderately entangled while the PtBS-16 chains ($M_{PtBS} = 16.4 \times 10^3 \cong 0.4M_{e,bulk}^{PtBS}$) are not entangled in respective bulk systems, as can be also noted from the ω dependence of their moduli; cf. cross of the G' and G'' curves seen in Figure 1 and the Rouse/Zimm-like shape of the curves seen in Figure 2. The steady state compliance of PI-20, $J_e = [G'/\{G''\}^2]_{\omega\to 0} = 0.42 \times 10^{-5}$ Pa^{-1}, was a little smaller than that of highly entangled PI ($J_e^\infty = 1.1 \times 10^{-5}$ Pa^{-1} at 30 °C[26]) but the dielectric relaxation time of PI-20, $\tau_\epsilon = 6.7 \times 10^{-4}$ s (evaluated from ϵ peak frequency) was well described by an empirical equation in the entangled range of $10^{-3}M = 10-300$ ($\tau_\epsilon = 6.2 \times 10^{-19}M^{3.5}$ s at 30 °C,[15,27] shifted from 40 °C with the aid of eq 1), which

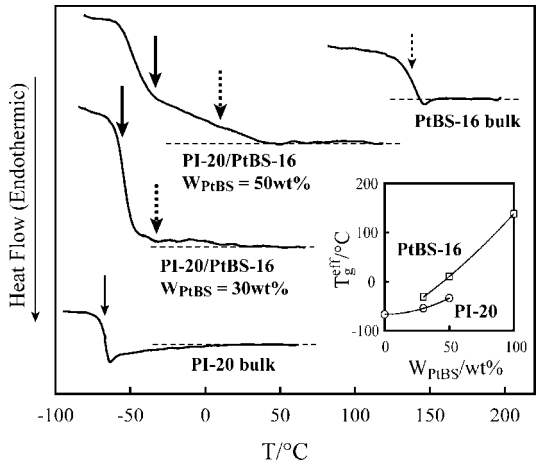

Figure 3. DSC traces for PI-20/PtBS-16 blends and bulk PI-20 and PtBS-16 systems. Thin solid and dotted arrows indicate T_g of bulk PI-20 and PtBS-16 (−67 and +138 °C), respectively. Thick solid and dotted arrows attached to the DSC traces denote effective T_g of PI-20 and PtBS-16 in the blends expected from WLF analysis of the dielectric and viscoelastic data of the blends. The inset shows plots of the effective T_g against w_{PtBS}. For further details, see text.

also demonstrates the moderately entangled character of bulk PI-20.

The lack of entanglement (or motional constraint) for the PtBS-16 chain, noted in the bulk state, is not necessarily an intrinsic property of this low-*M* chain but may be affected on blending with PI-20. Correspondingly, the motional constraint for PI-20 may be also affected on blending. These points are later discussed for the viscoelastic and dielectric data of the PI-20/PtBS-16 blends.

3.2. Overview of Behavior of PI-20/PtBS-16 Blends. Figure 3 shows the DSC profiles measured for the PI-20/PtBS-16 blends with w_{PtBS} = 30 and 50 wt %. For comparison, the profiles are shown also for bulk PI-20 and PtBS-16. The dashed lines indicate the high-*T* baselines, and thin solid and dotted arrows indicate the glass transition temperatures T_g for bulk PI-20 and bulk PtBS-16, respectively ($T_{g,bulk}^{PI}$ = −67 °C and $T_{g,bulk}^{PtBS}$ = 138 °C, chosen as the middle-point temperatures for respective glass transition zones). The thick solid and dotted arrows indicate *effective* T_g for PI-20 and PtBS-16 in the blends expected from the WLF analysis explained later, and the inset shows plots of the effective T_g against w_{PtBS}. We note that the blends exhibit broad, almost two-step glass transition (in particular at w_{PtBS} = 50 wt %) at temperatures close to these effective T_g, despite their *static* homogeneity explained earlier. This broad glass transition reflects the dynamic heterogeneity affecting the segmental dynamics in the blends, as noted for a variety of miscible blends.[1−11]

Figures 4 and 5 show the viscoelastic and dielectric data measured for the PI-20/PtBS-16 blends with w_{PtBS} = 30 and 50 wt %, respectively. The raw dielectric loss (ϵ'') data are multiplied by a factor of 10^3 and compared with the storage and loss moduli (G' and G'') data. For clarity of the figures, the data are shown only at representative temperatures.

Since PtBS-16 has no type-A dipole, the dielectric relaxation of the blends detected through the ϵ'' data are exclusively attributed to the global motion of the PI-20 chains therein. In Figures 4 and 5, the terminal dielectric relaxation characterized by the power-law tail, $\epsilon'' \propto \omega$, is clearly observed without disturbance from the direct current (dc) conduction due to ionic impurities giving $\epsilon_{dc}'' = \sigma/\omega \propto \omega^{-1}$ (with σ = dc conductivity). In fact, the dc contribution to the ϵ'' data was observed at high *T*; see the dashed line attached to the ϵ'' data at 100 °C shown in Figure 4. However, even for this case, the dielectric relaxation

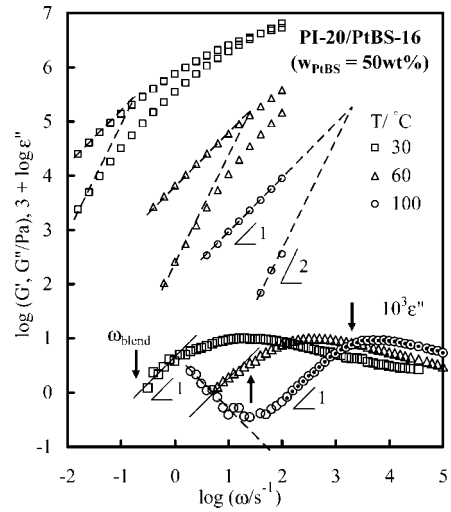

Figure 4. Viscoelastic and dielectric behavior of PI-20/PtBS-16 blend with w_{PtBS} = 50 wt % at representative temperatures as indicated. The arrows indicate the average viscoelastic relaxation frequency of the blend, ω_{blend}. As for the dielectric data at 100 °C, large unfilled circle, dashed line (of slope = −1), and small filled circles indicate the raw ϵ'' data, the direct current (dc) contribution ϵ_{dc}'', and the residue $\epsilon'' - \epsilon_{dc}''$, respectively. For further details, see text.

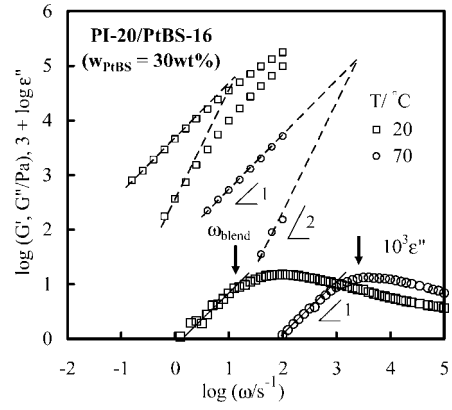

Figure 5. Viscoelastic and dielectric behavior of PI-20/PtBS-16 blend with w_{PtBS} = 30 wt % at representative temperatures as indicated. The arrows indicate the average viscoelastic relaxation frequency of the blend, ω_{blend}.

is completed at relatively high ω, where the dc contribution is negligibly small. Thus, throughout this paper, only the raw ϵ'' data having negligible dc contribution are utilized for discussing the PI-20 global dynamics in the blends. The quality of those raw ϵ'' data was checked in the following way. Whenever the dc contribution was detected at high *T*, we allowed changes of σ by ± 30% to fit the low-ω ϵ'' data with $\epsilon_{dc}'' = \sigma/\omega$, subtracted this ϵ_{dc}'' from the raw ϵ'' data, and compared the residue $\epsilon'' - \epsilon_{dc}''$ with the raw data. At moderately high ω, the residue was quite insensitive to the ± 30% changes of σ and indistinguishable from the raw data; compare small filled circles (residue) and large unfilled circles (raw data) shown in Figure 4. We utilized only the raw data at such moderately high ω where the terminal behavior was readily detected.

As seen in Figures 4 and 5, the blends as a whole (almost) exhibit the terminal viscoelastic relaxation characterized by the power-law tails of their storage and loss moduli data, $G_B' \propto \omega^2$ and $G_B'' \propto \omega$ (cf. dashed lines attached to the low ω data). From these tails, we can evaluate the second-moment average viscoelastic relaxation frequency[28] of the blends defined by

$$\omega_{\text{blend}} = \left[\frac{\omega G_B'}{G_B''}\right]_{\omega\to 0} \quad (3)$$

For monodisperse linear PI chains (in an iso-frictional state), the similarly defined second-moment average *dielectric* relaxation frequency, $[\omega\epsilon''/\{\epsilon_0 - \epsilon'\}]_{\omega\to 0}$ with ϵ_0 and ϵ' respectively being the static and dynamic dielectric constants, agrees well with the angular frequency $\omega_{\epsilon\text{-peak}}$ for the ϵ'' peak[15,27] and the viscoelastic and dielectric second-moment average relaxation frequencies are close to each other.[27,29,30] Thus, we can compare the viscoelastic ω_{blend} and dielectric ϵ'' data of the blends (Figures 4 and 5) to specify the fast component therein. At low T, ω_{blend} (shown with the solid arrows) is located at low frequencies where the ϵ'' data are proportional to ω and the global relaxation of PI-20 has completed. This fact unequivocally indicates that PI-20 relaxes faster than the blend as a whole and thus PI-20 and PtBS-16 are the fast and slow components in the blends with $w_{\text{PtBS}} = 30$ and 50 wt % at those T. However, ω_{blend} approaches $\omega_{\epsilon\text{-peak}}$ and the difference of the terminal relaxation frequencies of PI-20 and PtBS-16 becomes smaller with increasing T. (Consequently, the PI-20 relaxation would become slower than the PtBS-16 relaxation at higher T not tested in this study.) In the PI-20/PtBS-16 blend with smaller w_{PtBS} (=20 wt %), ω_{blend} agreed well with $\omega_{\epsilon\text{-peak}}$ in a range of T between 30 and 70 °C and thus PI-20 was the slow component, as found in the previous study.[20] These changes of the relative relaxation rates of PI-20 and PtBS-16 strongly influence the thermo-rheological behavior of the PI-20 chains in the blends, as discussed below.

3.3. Dynamic Behavior of PI Chains in Blends. *3.3.1. Thermo-Rheological Behavior of PI.* Figure 6 shows the master curves of the ϵ'' data measured for the PI-20/PtBS-16 blends with $w_{\text{PtBS}} = 30$ and 50 wt %; cf. top two panels. The data at respective temperatures T are multiplied by an intensity correction factor,[31] $b_T = T/T_r$ with T and T_r being represented in K unit, and shifted along the ω axis by a factor of a_T to achieve the best superposition around the ϵ'' peak with the data at a reference temperature T_r: T_r was chosen to be 343 and 393 K (70 and 120 °C) for $w_{\text{PtBS}} = 30$ and 50 wt %, respectively. (A change of the density, much smaller than the change of T (in K) itself, has been safely neglected in this b_T factor as well as the $b_T°$ factor explained below.[31]) For comparison, the master curve (with $T_r = 30$ °C) is also shown for the blend with $w_{\text{PtBS}} = 20$ wt % examined in the previous work.[20] The a_T data for these blends are summarized in Figure 7.

In all panels of Figure 6, the solid curve represents the normalized dielectric loss of bulk PI-20 at $T_{r,\text{bulk}} = 303$ K (30 °C), $\phi_{\text{PI}} b_T° \epsilon_{\text{PI,bulk}}''(\omega/\Lambda)$, plotted against ω; see Figure 1 for the raw $\epsilon_{\text{PI,bulk}}''$ data. Here, ϕ_{PI} is the volume fraction of PI in the blends, and $b_T° = T_{r,\text{bulk}}/T_r$ with T_r being the reference temperature of PI-20 in the blends; (ϕ_{PI}, T_r/K) = (0.53, 393), (0.73, 343), and (0.81, 303) for $w_{\text{PtBS}} = 50$, 30, and 20 wt %. The frequency reduction factor Λ (=7.3, 2.0, and 0.44 for $w_{\text{PtBS}} = 50$, 30, and 20 wt %) was chosen to give the best superposition of the $\phi_{\text{PI}} b_T° \epsilon_{\text{PI,bulk}}''(\omega/\Lambda)$ data on the ϵ'' peaks of the blends.

At low T, the dielectric mode distribution of PI-20 in the blends with $w_{\text{PtBS}} = 50$ and 30 wt % agrees with that of bulk PI-20 at $\omega \geq \omega_{\epsilon\text{-peak}}$ but broadens at lower ω; see Figure 6. This low-ω mode distribution narrows with increasing T and finally coincides with that of bulk PI-20 at sufficiently high T, demonstrating the thermo-rheological complexity of the PI-20 chains in the blends. This behavior strongly suggests that the PI-20 chains split into the majority and minority components, the former governing the observed ϵ'' peak and relaxing faster than the latter, and that the difference of the relaxation rates of these components decreases with increasing T.[18] This difference appears to be sufficiently small in the entire range of T examined for the blend with $w_{\text{PtBS}} = 20$ wt % (bottom panel), which possibly led to the thermo-rheological simplicity seen at those T.

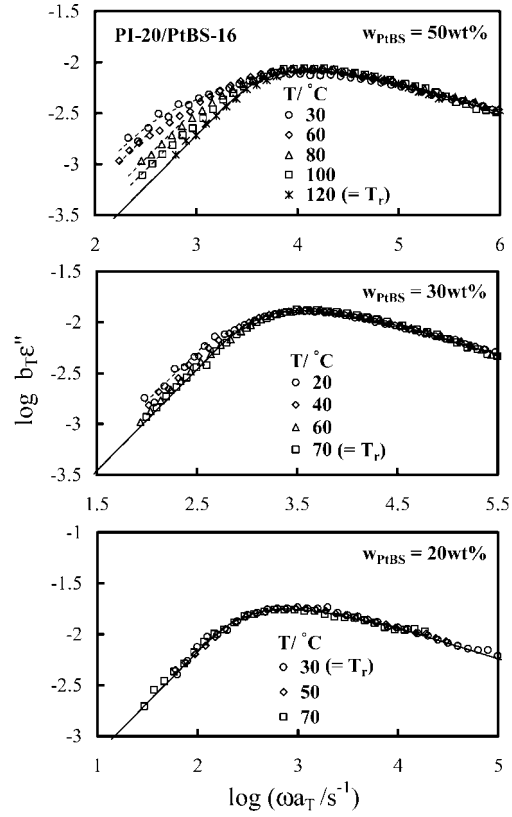

Figure 6. Test of time−temperature superposability for the ϵ'' data of PI-20/PtBS-16 blends with $w_{\text{PtBS}} = 50$ wt %, 30 wt %, and 20 wt %. The ϵ'' data are multiplied by an intensity correction factor $b_T = T/T_r$ and shifted along the ω axis by a factor of a_T to superimpose their ϵ'' peak onto the peak at the reference temperature T_r as indicated. The solid curves indicate the normalized dielectric data of bulk PI-20 plotted against a reduced frequency ω/Λ. For further details, see text. The data of PI-20/PtBS-16 blend with $w_{\text{PtBS}} = 20$ wt % were taken from ref 20.

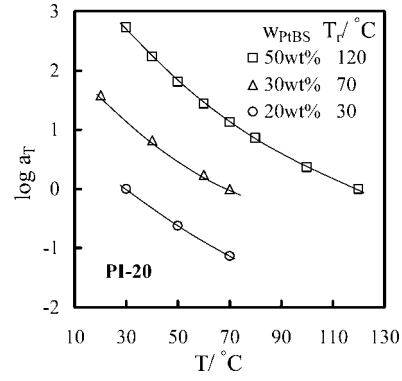

Figure 7. Plots of the time−temperature shift factor a_T of ϵ'' data (shown in Figure 6) against the temperature T.

The splitting of the PI-20 chains into the majority and minority, seen at $w_{\text{PtBS}} = 30$ and 50 wt %, can be related to the frictional nonuniformity due to the PtBS-16 chains (that relax more slowly even compared to the minority PI-20 at low T where the splitting/mode broadening is observed). This effect of PtBS-16 on the PI-20 relaxation is further discussed later in

Figure 10 in relation to the terminal relaxation times of PI-20 and PtBS-16 in the blends.

3.3.2. Separate Examination of Behavior of Majority and Minority PI. Here, we attempt to factorize the ϵ'' data of the blends into contributions from the majority and minority components of PI-20 therein and examine the relaxation behavior of respective components. It is well-known that the dielectric mode distribution for the global relaxation (end-to-end vector fluctuation) of PI chains is insensitive to their molecular weight and changes of the environment (e.g., dilution with a solvent) unless they are subjected to strong thermodynamic/spatial confinements.[15,32] Thus, we can safely approximate that the dielectric mode distribution (observed as the relative ω dependence of ϵ'') is the same for each component in the blends and bulk PI-20. Then, the $\epsilon''(\omega,T)$ data of the blends at a given T can be expressed in terms of the $\epsilon_{\mathrm{PI,bulk}}''(\omega)$ data of bulk PI-20 at its reference temperature, $T_{\mathrm{r,bulk}} = 303$ K, as[31]

$$\varepsilon''(\omega,T) = b_T'\,\phi_{\mathrm{PI}}[v_{\mathrm{fast}}\epsilon_{\mathrm{PI,bulk}}''(\omega/\lambda_{\mathrm{fast}}) + \{1-v_{\mathrm{fast}}\}\epsilon_{\mathrm{PI,bulk}}''(\omega/\lambda_{\mathrm{slow}})] \quad (4)$$

with $b_T' = T_{\mathrm{r,bulk}}/T$. ϕ_{PI} is the PI-20 volume fraction in the blend, λ_{fast} and λ_{slow} are the frequency reduction factors for the fast and slow components of PI-20 (majority and minority), respectively, and v_{fast} is the fast component fraction in the ensemble of PI-20 chains.

Here, a comment needs to be added to eq 4. In general, $\epsilon''(\omega,T)$ is written as a sum of the contributions from more than two components. However, the close coincidence of the ϵ'' data of the blends and bulk PI-20 seen at $\omega \geq \omega_{\epsilon\text{-peak}}$ (Figure 6) suggests that the data of the blends at those ω are dominated by a single fast component (majority). Furthermore, the ϵ'' data of the blends at lower ω were larger than the bulk data only by a factor <5 (because of this coincidence at $\omega \geq \omega_{\epsilon\text{-peak}}$), which did not allow us to finely resolve the slower components contributing to the blend data at $\omega < \omega_{\epsilon\text{-peak}}$. For this reason, we considered a *representative* slow component as a minority and tested the validity of eq 4. In fact, the ϵ'' data of the blends were successfully described by eq 4 within experimental uncertainty, as explained below. Thus, in what follows, we keep this representative character of the minority in our mind to discuss the changes of the relaxation times and fractions of the majority and minority with temperature.

We attempted to fit the blend data with eq 4 and determine the three parameters therein, λ_{fast}, λ_{slow}, and v_{fast}, in the following way: Since the ϵ'' data of the blend and bulk PI-20 are close to each other at $\omega \geq \omega_{\epsilon\text{-peak}}$ (cf. Figure 6), λ_{fast} should be close to the Λ/a_T ratio with Λ and a_T being the frequency reduction factor "utilized in" Figure 6 and the shift factor shown in Figure 7, respectively. The close coincidence of the blend and bulk data also indicates that v_{fast} is close to a ratio r_ϵ of the ϵ'' peak height of the blend to that of bulk PI-20 (after the correction of the PI volume fraction and temperature). Thus, in the fitting procedure, λ_{fast} and v_{fast} were varied from the known values of Λ/a_T and r_ϵ in a stepwise way; a few percent change for either λ_{fast} or v_{fast} in each step and less than 30% change in total (after several steps). For each step, we examined if the blend data can be fitted by eq 4 utilizing the $\epsilon_{\mathrm{PI,bulk}}''$ data of bulk PI and the given λ_{fast} and v_{fast} values in this step together with an appropriately chosen λ_{slow} value. Indeed, good fit was achieved for λ_{fast} and v_{fast} close to Λ/a_T and r_ϵ, respectively, and λ_{slow} smaller than λ_{fast}; for example, $\lambda_{\mathrm{fast}} = \Lambda/a_T$ ($= 0.042$), $v_{\mathrm{fast}} = 0.73r_\epsilon$ ($= 0.66$), and $\lambda_{\mathrm{slow}} = 0.14\lambda_{\mathrm{fast}}$ ($= 0.006$) for the blend with $w_{\mathrm{PtBS}} = 50$ wt % at 40 °C. (The fitting required us to just vary the single parameter λ_{slow} in a wide range and thus included no significant ambiguity.)

Figures 8 and 9, respectively, show the best-fit results thus obtained for the blends with $w_{\mathrm{PtBS}} = 50$ and 30 wt %. The dotted and dashed curves show the contributions from the fast and slow components of PI-20, respectively, and the solid curves indicate the sum of these contributions (eq 4). This sum agrees well

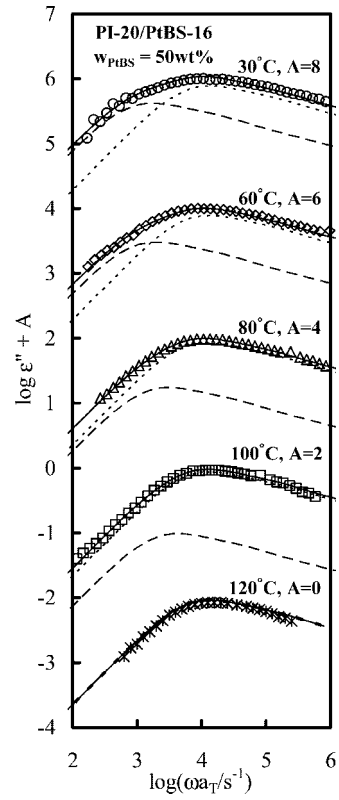

Figure 8. Decomposition of raw ϵ'' data of PI-20/PtBS-16 with $w_{\mathrm{PtBS}} = 50\%$ (symbols) into contributions from the majority (dotted curves) and minority (dashed curves) of PI-20 chains in the blends. The minority relaxes slowly compared to the majority. Solid curves indicate the sum of these contributions. For clarity of Figure, the data and curves at different temperatures (plotted against ωa_T with a_T given in Figure 7) are shifted vertically by the factors A as indicated.

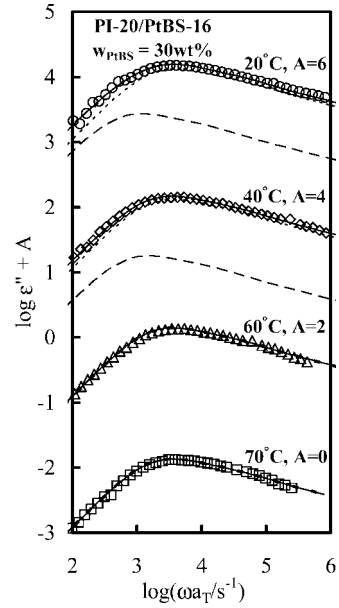

Figure 9. Decomposition of raw ϵ'' data of PI-20/PtBS-16 with $w_{\mathrm{PtBS}} = 30\%$ (symbols) into contributions from the majority (dotted curves) and minority (dashed curves) of PI-20 chains in the blends. The minority relaxes slowly compared to the majority. Solid curves indicate the sum of these contributions. For clarity of Figure, the data and curves at different temperatures (plotted against ωa_T with a_T given in Figure 7) are shifted vertically by the factors A as indicated.

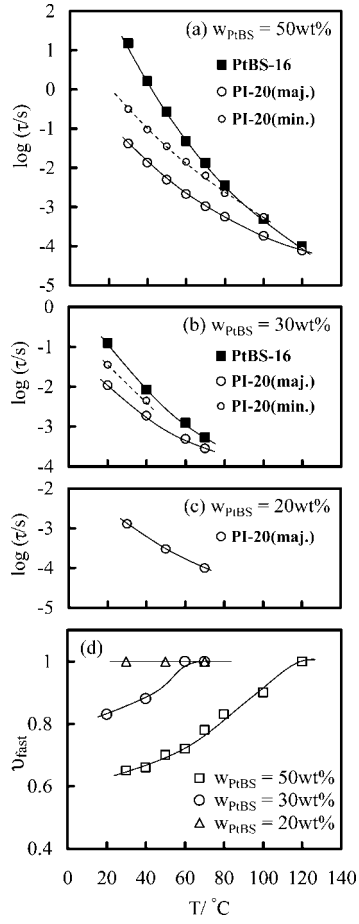

Figure 10. Top three panels: Temperature dependencies of dielectric relaxation times of the majority and minority of PI-20 chains (large and small circles) and viscoelastic relaxation time the PtBS-16 chains (filled squares) in PI-20/PtBS-16 blends with the PtBS concentrations w_{PtBS} as indicated. Bottom panel: Plots of the fraction of the majority of PI-20 chains in the blends against temperature T. The curves are guide for eye.

with the $\epsilon''(\omega,T)$ data (symbols), which demonstrates that the PI-20 chains in the blends can be classified into the fast component (majority) and the slow component (minority), with the latter being the representative of various slow components.

From the frequency reduction factors λ_{fast} (almost identical to Λ/a_T) and λ_{slow} determined from the fitting, the dielectric relaxation time of PI-20 in the blends was evaluated as

$$\tau_\epsilon = \{\omega_{\epsilon\text{-peak}}^{bulk}\lambda_j\}^{-1} \quad (5)$$

where j = fast (majority) and slow (minority), and $\omega_{\epsilon\text{-peak}}^{bulk}$ ($= 1.5 \times 10^3$ s^{-1}) is the angular frequency for the ϵ'' peak of bulk PI-20 at its $T_{r,bulk}$ (= 30 °C). Top three panels of Figure 10 show plots of the τ_ϵ data of the majority and minority components of PI-20 in the blends against the temperature T; cf. large and small circles. The bottom panel shows the plots of the majority fraction υ_{fast} (determined from the fitting together with λ's). For the blend with w_{PtBS} = 20 wt %, the ϵ'' data exhibited the thermo-rheological simplicity and their mode distribution was indistinguishable from that of bulk PI-20; cf. bottom panel of Figure 6. Thus, for this blend, υ_{fast} was set to be unity and τ_ϵ was evaluated only for the majority.

In the top two panels of Figure 10, large filled squares indicate the viscoelastic relaxation time of the PtBS-16 chains with w_{PtBS} = 50 and 30 wt % evaluated from their modulus G_{PtBS}*, $\tau_{G,PtBS} = [G_{PtBS}'/\omega G_{PtBS}'']_{\omega\to 0}$. G_{PtBS}* was obtained by subtracting the modulus G_{PI}* of the PI-20 chains in the blends from G_B* of the blends as a whole, as explained later in detail. (For the blends with w_{PtBS} = 20 wt %, G_{PI}* was very close to G_B* and this subtraction could not be made accurately.[20] For this reason, no $\tau_{G,PtBS}$ data are shown in the third panel.)

Table 2. Degree of Overlapping and Iso-ζ Temperature of the Components in Blends and Bulk

	w_{PtBS}	C_{PtBS}/C_{PtBS}*	$T_{iso\text{-}PI}$/°C	$T_{iso\text{-}PtBS}$/°C
PI-20/PtBS-16	50%	2.3	63	43
PI-20/PtBS-16	30%	1.4	42	1
PI-20/PtBS-16[a]	20%	0.9	41	
PI-20 (bulk)			30[b]	
PtBS-16 (bulk)				171[b]

[a] $T_{iso\text{-}PtBS}$ could not be determined for the PI-20/PtBS-16 blend with w_{PtBS} = 20% because the modulus of PtBS-16 in this blend was not obtained with acceptable accuracy.[20] [b] For bulk PI-20 and PtBS-16, the reference temperatures of the master curves (Figures 1 and 2) were chosen to be T_{iso}. The local friction at respective T_{iso} is much larger (the difference $T_{iso} - T_g$ is much smaller) for bulk PtBS-16 than for bulk PI-20.

In the blends with w_{PtBS} = 30 and 50 wt %, the viscoelastic $\tau_{G,PtBS}$ of PtBS-16 is considerably longer than the dielectric τ_ϵ of the coexisting PI-20 at most of the temperatures examined (cf. top two panels of Figure 10), confirming that PtBS-16 and PI-20 are the slow and fast components therein. Furthermore, the PI-20 chains in the PI/PtBS blends should have $\tau_G \cong \tau_\epsilon/2$ at high T where the difference of the PI-20 and PtBS-16 relaxation rates is reduced, as similar to the behavior of bulk monodisperse PI systems in which all chains relax at the same rate.[27,28,33] (The PI chains in the monodisperse systems relax partly through the dynamic tube dilation (DTD) mechanism to have $\tau_G \cong \tau_\epsilon/2$.[27,28,33]). The difference of the relaxation rates of the PtBS-16 and PI-20 chains in the PI/PtBS blends is more significant than it appears in Figure 10, given that the τ_G/τ_ϵ ratio for PI-20 ($\cong 1/2$ at high T) is taken into account.

3.3.3. Origin of Thermo-Rheological Complexity of PI. The PI-20/PtBS-16 blends with w_{PtBS} = 30 and 50 wt % satisfy the conditions explained earlier: (1) The concentration C_{PtBS} of PtBS-16 (the slow chain) is not much larger than its overlapping concentration C_{PtBS}*; C_{PtBS}/C_{PtBS} * ≤ 2.3 as shown in Table 2. (2) The average end-to-end distance R_{PI} of PI-20 (the fast chain) is not much larger than R_{PtBS} of PtBS-16; $R_{PI}/R_{PtBS} \cong 1.6$ as shown in Table 1. (3) PI-20 and PtBS-16 have widely separated bulk T_g (Figure 3), which leads to a difference of their effective T_g in the blends and to the corresponding difference of their local friction coefficients. Thus, the dynamic heterogeneity of the PtBS concentration should be effectively frozen over the length scale of R_{PI} ($\sim R_{PtBS}$) in the time scale of the global relaxation of PI-20, which naturally results in the splitting of the PI-20 chains into the majority and minority components. The minority should be in the transiently PtBS-enriched region to have a higher effective T_g and feel a higher friction compared to the majority, which leads to the observed difference of their τ_ϵ and mode broadening at low T. Since the acceleration of the relaxation with T would be stronger for the minority component having the higher effective T_g (as expected from the WLF equation for a_T utilizing T_g as a reference temperature[22]), the whole ensemble of the PI-20 chains should exhibit the thermo-rheological complexity and its mode distribution approaches that of bulk PI-20 at high T, which is in harmony with the observation. In addition, the majority fraction increases with increasing T (cf. bottom panel of Figure 10), which also contributes to this complexity. (This increase of the majority fraction may be partly due to the decrease of the difference between the relaxation times of PtBS-16 and the minority PI-20; cf. top two panels of Figure 10: This decrease enhances a probability for the escape of the minority PI-20 chains from the PtBS-rich region before completion of their global relaxation. Then, some of the PI chains behaving as the minority at low T would become indistinguishable from the majority (defined as

the component governing the ϵ'' peak), which possibly results in the increase of the majority fraction.)

All above results confirm the molecular scenario proposed in the previous work.[18] In relation to this point, we should emphasize that the PI-20 chains in the blend with $w_{PtBS} = 20$ wt % exhibit thermo-rheological simplicity (cf. Figure 6) because they relax more slowly than the coexisting PtBS-16 chains.[20] This simplicity corresponds to the high-T asymptotic behavior seen for larger w_{PtBS}. It is informative to consider why PI-20 behaves as the slow component at $w_{PtBS} = 20$ wt %. The glass transition zone of the blend becomes narrower with decreasing w_{PtBS}, suggesting that the difference of the effective T_g of PI-20 and PtBS-16 significantly decreases with decreasing w_{PtBS} due to the strong plasticization of PtBS-16 by PI-20; cf. Figure 3. In the blend with $w_{PtBS} = 20$ wt %, PI-20 and PtBS-16 seem to have rather similar effective T_g values. (In fact, no broad glass transition was clearly detected in DSC measurements for this blend.) Then, the PtBS-16 chains relax faster than PI-20 just because of their low M_{PtBS} value ($<M_{PI}$), thereby smearing the frictional nonuniformity for the global relaxation of PI-20 at $T = 30-70$ °C and allowing PI-20 to exhibit the thermo-rheological simplicity. This argument is consistent with the observation that the simplicity vanishes in the same range of T when PI-20 is blended with a *high-M* PtBS-70 at the same composition ($w_{PtBS} = 20$ wt %).[18] The *high-M* PtBS-70 chains relaxed more slowly than PI-20 even when PI-20 and PtBS-70 have rather similar effective T_g values (at $w_{PtBS} = 20$ wt %), thereby forcing PI-20 to violate the simplicity.

3.3.4. Further Discussion of Dynamics of Majority PI in the Iso-Frictional State. At a given T, the PI-20 relaxation in the PI-20/PtBS-16 blends with $w_{PtBS} = 30$ and 50 wt % is slower than that in the bulk PI-20 system. This difference of the PI-20 relaxation rates in the blends and bulk should emerge through several different mechanisms. First of all, the PI-20 chains are antiplasticized by the PtBS-16 chains (cf. Figure 3) to have the local friction coefficient ζ larger than that in the bulk PI-20 system at the same T. Furthermore, the dynamic tube dilation (DTD)/constraint release (CR) mechanism[27,28,33] working in the moderately entangled bulk PI-20 system should be restricted by the PtBS-16 chains to retard the PI-20 relaxation compared to that in the bulk system, given that the PtBS-16 chains are concentrated and relaxing much more slowly than the PI-20 chains. (Data showing the effect of this restriction on the component relaxation in homopolymer blends are summarized in Appendix A.) In addition, even in the iso-ζ state, the PI-20 chain may feel some motional constraint due to such slow PtBS-16 chains, i.e., the Rouse motion of the PI-20 chain within its entanglement segment may be constrained by the PtBS-16 chains. The shift factor a_T (Figure 7) obtained for the majority of the PI-20 chains in the PI-20/PtBS-16 blends should reflect all of these effects. In other words, a_T for the PI-20 chains in the PI/PtBS blends is not identical to the $\zeta(T)/\zeta(T_r)$ ratio. This feature is qualitatively different from the feature of homopolymer systems simply having $a_T = \zeta(T)/\zeta(T_r)$.

In the following subsections, we first make a correction of the a_T data of PI-20 in the PI-20/PtBS-16 blends for the restriction of DTD/CR. This correction is minor in a numerical sense but is important conceptually. Then, WLF analysis is made for the a_T data corrected for this restriction to determine an iso-frictional (iso-ζ) temperature $T_{iso\text{-}PI}$ for PI-20. Finally, the dielectric τ_ϵ data of PI-20 in the blends and bulk at $T_{iso\text{-}PI}$ are compared to discuss an effect of PtBS-16 chains on the motion of PI-20 chains in the iso-ζ state. Readers not interested in details of the correction of a_T and determination of $T_{iso\text{-}PI}$ may skip subsections 3.3.4.1 and 3.3.4.2 and directly proceed to subsection 3.3.4.3 where the effect of PtBS-16 is discussed on the basis of the τ_ϵ data.

Here, a few comments need to be added for the iso-ζ correction through the WLF (or Vogel-Fulcher) analysis that basically scales the *local friction* ζ of polymer chains as a function of a distance $T - T_r$ from a reference temperature T_r. A reviewer for this paper argued that the iso-ζ correction is to be made by utilizing a normalized temperature T/T_g that determines the cooperative segmental dynamics in the vicinity of T_g (glassy dynamics reflecting the fragility),[34−36] rather than $T - T_r$, and that the correction cannot be made through the WLF analysis because of the difference of the T dependencies of the glassy (segmental) and rubbery (global) relaxation times. Indeed, this difference is the origin of the thermo-rheological complexity of bulk homopolymers in the *rubber-to-glass* transition zone (at low T) where the glassy and rubbery relaxation occurs simultaneously.[14,29,37−39] However, the rubbery relaxation itself exhibits the thermo-rheological simplicity even in this zone, as suggested from rheo-optical resolution of the two relaxation processes.[37,38] Furthermore, the difference of the T dependencies of the glassy and rubbery relaxation times vanishes and both times exhibit the *same WLF-type T dependence* at high T.[14,29,37−39] The viscoelastic/dielectric data of the blends presented in this study reflect the rubbery relaxation of the component chains at such *high T* (well above the effective T_g in the blends; cf. Figure 3), and the motional unit for this relaxation is the *Rouse segment*[22,37,38] not related to the glassy dynamics in the vicinity of T_g, which is consistent with a difference of the fragilities for the glassy and rubbery relaxation processes found in a recent study.[39] Consequently, for those data, the local friction ζ is appropriately corrected through the standard WLF analysis[22] explained in Appendix B. This is the case not only for the PI-20 relaxation examined below but also for the PtBS-16 relaxation discussed in a later section.

3.3.4.1. Correction of a_T for Restriction of DTD/CR. Relaxation time data obtained for binary blends of low-M and high-M PI chains are free from the antiplasticization effect and thus helpful for making the correction for the restriction of DTD/CR on blending. Specifically, increases of the viscoelastic and dielectric relaxation times $\tau_{G1}(\phi_2)$ and $\tau_{\epsilon 1}(\phi_2)$ of the fast component 1 (low-M PI), resulting from this restriction due to the slow component 2 (high-M PI having the volume fraction ϕ_2), was found to be well correlated with a ratio of the viscoelastic relaxation times of the two components in the blend, $\tau_{G2}(\phi_2)/\tau_{G1}(\phi_2)$; see Appendix A. At this moment, no DTD/CR theory describing this correlation accurately and enabling the above correction rigorously is available. Thus, we make this correction by utilizing empirical equations (Appendix A) that satisfactorily quantify the correlation

$$\log\left(\frac{\tau_{G1}(\phi_2)}{\tau_{G1}(0)}\right) = B\tanh\left\{\alpha\left[\log\left(\frac{\tau_{G2}(\phi_2)}{\tau_{G1}(\phi_2)}\right)\right]^q\right\} \tag{6}$$

$$Q \equiv \left(\frac{\tau_{\epsilon 1}(\phi_2)}{\tau_{\epsilon 1}(0)}\right) = \left(\frac{\tau_{G1}(\phi_2)}{\tau_{G1}(0)}\right)^{0.3} > 1 \tag{7}$$

Here, $\tau_{G1}(0)$ and $\tau_{\epsilon 1}(0)$ denote the viscoelastic and dielectric relaxation times of the fast component in its monodisperse state, and the coefficients (B, α, q) are (0.2, 0.23, 3) and (0.41, 0.2, 2.5) for $\phi_2 = 0.27$ and 0.47, respectively. Note that the dielectric relaxation of PI in the monodisperse state is hardly affected while the viscoelastic relaxation is considerably accelerated (by a factor $\cong 2$) by the DTD mechanism.[27,33] For this reason, the restriction of DTD for the fast component in the blends increases $\tau_{\epsilon 1}(\phi_2)$ less significantly than $\tau_{G1}(\phi_2)$; namely, a relationship $\tau_{\epsilon 1}(\phi_2)/\tau_{\epsilon 1}(0) < \tau_{G1}(\phi_2)/\tau_{G1}(0)$ holds. The empirical exponent of 0.3 (<1) appearing in eq 7 is a consequence of this relationship.

The factor Q given by eq 7 specifies the increase of the dielectric τ_ϵ of the fast component due only to the restriction of

DTD/CR. We may apply eqs 6 and 7 to our PI-20/PtBS-16 blends to evaluate Q for the PI-20 chains (fast component therein) and then correct their raw a_T data (Figure 7) for this restriction due to PtBS-16; the corrected shift factor a_T^{cor} is given by a_T/Q. For this purpose, the viscoelastic relaxation time of the slow component (PtBS-16) in our blends, $\tau_{G2}(\phi_2)$ appearing in eq 6, can be well approximated by $\tau_{GB}(\phi_2)$ of the blend as a whole (that was directly obtained from the viscoelastic data shown in Figures 4 and 5.) Although $\tau_{GB}(\phi_2)$ should be somewhat smaller than $\tau_{G2}(\phi_2)$ in a rigorous sense, the Q values obtained from the following analysis changed less than a few percent even if we artificially increased $\tau_{GB}(\phi_2)$ by a factor of 2. Thus, this approximation was quite harmless, allowing us to replace the $\tau_{G2}(\phi_2)/\tau_{G1}(\phi_2)$ term in eq 6 by

$$\frac{\tau_{G2}(\phi_2)}{\tau_{G1}(\phi_2)} \cong \frac{\tau_{GB}(\phi_2)}{\tau_{G1}(\phi_2)} = \left\{\frac{\tau_{GB}(\phi_2)}{\tau_{\epsilon 1}(\phi_2)}\right\} \times \left\{\frac{\tau_{\epsilon 1}(\phi_2)}{\tau_{G1}(\phi_2)}\right\} = \left\{\frac{\tau_{GB}(\phi_2)}{\tau_{\epsilon 1}(\phi_2)}\right\} \times \left\{\frac{\tau_{\epsilon 1}(0)}{\tau_{G1}(0)}\right\} \times Q^{-2.33} \quad (8)$$

(A relationship obtained from rearrangement of eq 7, $\tau_{\epsilon 1}(\phi_2)/\tau_{G1}(\phi_2) = Q^{-2.33}\tau_{\epsilon 1}(0)/\tau_{G1}(0)$, has been utilized in eq 8.) Inserting eqs 7 and 8 into eq 6, we find an equation that expresses Q only in terms of directly measureable quantities,

$$\log Q = 0.3B \tanh\left\{\alpha\left[\log\left(\frac{\tau_{GB}(\phi_2)}{\tau_{\epsilon 1}(\phi_2)}\right) + \log\left(\frac{\tau_{\epsilon 1}(0)}{\tau_{G1}(0)}\right) - 2.33 \log Q\right]^q\right\} \quad (9)$$

Substituting the known $\tau_{GB}(\phi_2)$ and $\tau_{\epsilon 1}(\phi_2)$ data (for $\phi_2 = \phi_{PtBS} = 0.27$ and 0.47) and the known $\tau_{\epsilon 1}(0)/\tau_{G1}(0)$ ratio ($\cong$2 for bulk PI-20) in eq 9 and utilizing the parameters (B, α, q) specified earlier, we numerically solved eq 9 to evaluate Q for the majority of PI-20 in the PI-20/PtBS-16 blends ($w_{PtBS} = 30$ and 50 wt %). Q was found to decrease from 1.31 to 1.01 with increasing T from 30 to 120 °C for $w_{PtBS} = 50$ wt %, and a less significant change was noted for $w_{PtBS} = 30$ wt %. These changes of Q are minor in a numerical sense (and neglected in the previous study for the PI-20/PtBS-70 blend with $w_{PtBS} = 20$ wt %[18]). However, the effect of the restriction of DTD/CR represented by Q is conceptually important and thus incorporated in the analysis in this paper.

3.3.4.2. Determination of Iso-ζ Temperature. For the shift factor corrected for the restriction of DTD/CR as above, $a_T^{cor} = a_T/Q$, we made the standard WLF analysis[22] explained in Appendix B to determine the iso-ζ temperature $T_{iso\text{-}PI}$ for the majority of PI-20 in the blends. These $T_{iso\text{-}PI}$ values, corresponding to $T_{iso\text{-}PI}$ (bulk) = 30 °C (=$T_{r,bulk}$) of bulk PI-20, are summarized in Table 2. (The WLF analysis for the raw a_T data gave *apparent* iso-ζ temperatures higher than those $T_{iso\text{-}PI}$ by a few degrees. This difference is numerically minor but conceptually important.)

We chose $T_{iso\text{-}PI}$ as a new reference temperature for the blend (cf. Appendix B) and re-evaluated the corresponding shift factor, $a_{T\text{-}iso}$, from the a_T^{cor} data. For the PI-20/PtBS-16 blends with $w_{PtBS} = 30$ and 50 wt %, $a_{T\text{-}iso}$ is plotted against $T - T_{iso\text{-}PI}$ in the top panel of Figure 11; cf. square and triangle. For comparison, $a_{T\text{-}iso}$ is also shown for the previously examined PI-20/PtBS-16 blend with $w_{PtBS} = 20$ wt % (cf. circle).[20] In this 20 wt % blend, PI-20 relaxed slower than PtBS-16 and thus $T_{iso\text{-}PI}$ (= 41 °C) was determined from the WLF analysis of the raw a_T data[20] (without the correction for the restriction of DTD/CR). The solid curve indicates the WLF eq 1 that excellently describes the a_T data for bulk PI-20 with $T_{iso\text{-}PI}$(bulk) = $T_{r,bulk}$ = 30 °C. The plots for the PI-20/PtBS-16 blends with $w_{PtBS} = 20-50$ wt % are indistinguishable from this solid curve,

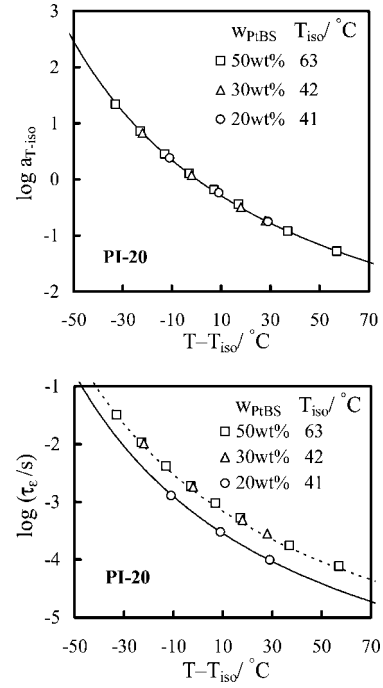

Figure 11. Top panel: Plots of the shift factor $a_{T\text{-}iso}$ of PI-20 in the PI-20/PtBS-16 blends with $w_{PtBS} = 20$, 30, and 50 wt % against a distance from the iso-ζ temperature, $T - T_{iso\text{-}PI}$. The iso-ζ state for PI-20 in the blends is defined with respect to bulk PI-20 at 30 °C. The solid curve indicates a_T of bulk PI plotted against $T - T_{r,bulk}$ with $T_{r,bulk} = 30$ °C (WLF eq 1). Bottom panel: Dielectric relaxation time τ_ϵ of the majority of PI-20 chains in the PI-20/PtBS-16 blends with $w_{PtBS} = 20$, 30, and 50 wt %. The τ_ϵ data are plotted against $T - T_{iso\text{-}PI}$. The solid curve indicates the τ_ϵ data of bulk PI-20 plotted against $T - T_{r,bulk}$ ($T_{r,bulk} = 30$ °C). The dotted curve shows the bulk τ_ϵ data multiplied by a factor of 2.4.

lending support to our WLF-determination of $T_{iso\text{-}PI}$ in the blends.

The above result allows us to regard the difference of the iso-ζ temperatures in the blends and bulk, $\Delta T_{iso} = T_{iso\text{-}PI}$(blend) − $T_{iso\text{-}PI}$(bulk), as a difference of the effective glass transition temperatures in these systems. Thus, we may utilize the ΔT_{iso} data to *estimate* the effective T_g of PI-20 in the blend as $T_{g,blend}^{PI} = T_{g,bulk}^{PI} + \Delta T_{iso}$ (with $T_{g,bulk}^{PI} = -67$ °C). These estimates, shown in Figure 3 with thick solid arrows attached to the DSC traces, are well located at the low-T side of the broad glass transition zone. This result lends further support to our WLF-determination of $T_{iso\text{-}PI}$.

3.3.4.3. Effect of PtBS-16 on the PI-20 Chain Motion in the Iso-ζ State. Here, we compare the terminal dielectric relaxation time τ_ϵ of the majority of the PI-20 chains in the blends with τ_ϵ of bulk PI-20 in the iso-ζ state. For this purpose, the raw τ_ϵ data for $w_{PtBS} = 30$ and 50 wt % (that are a little affected by the restriction of DTD/CR) are plotted against $T - T_{iso\text{-}PI}$ in the bottom panel of Figure 11; cf. square and triangle. For comparison, the τ_ϵ data in the previously examined PI-20/PtBS-16 blend with $w_{PtBS} = 20$ wt % are also shown; cf. circle. The solid curve indicates the $\tau_{\epsilon,bulk}$ data of bulk PI-20 plotted against $T - T_{iso\text{-}PI}$ (=$T - T_{r,bulk}$), and the dotted curve shows these bulk $\tau_{\epsilon,bulk}$ data multiplied by a factor of 2.4.

As noted for the plot shown in the bottom panel of Figure 11, τ_ϵ for the majority of PI-20 in the blends with $w_{PtBS} = 30$ and 50 wt % is larger than $\tau_{\epsilon,bulk}$ of iso-ζ bulk PI-20 by a factor of 2.4. The antiplasticization effect for PI-20 due to PtBS has been compensated in this iso-ζ plot, and the effect the restriction of DTD/CR on the PI-20 relaxation is too small to give the difference by a factor of 2.4: The Q factor representing this effect (cf. eqs 7 and 9) is smaller than 1.31 for the blends at all

T. Furthermore, τ_ϵ in the blend with $w_{PtBS} = 20$ wt % agrees with $\tau_{\epsilon,bulk}$ (cf. circles and solid curve), although this blend can be regarded, in the *simplest* case, as an entangled 80 wt % *solution* of PI-20 (PI volume fraction $\phi_{PI} = 0.81$) because PtBS-16 therein relaxed faster than PI-20.[20] For entangled PI solutions in an oligomeric solvent, experiments[33] indicated $\tau_\epsilon \propto \zeta\phi_{PI}^{\beta}$ with $\beta \cong 1.6$. Thus, in the simplest case, τ_ϵ for $w_{PtBS} = 20$ wt % is expected to be smaller than $\tau_{\epsilon,bulk}$ in the iso-ζ bulk by a factor of $0.81^{1.6} = 0.71$, which is large enough to be resolved in the plot shown in the bottom panel of Figure 11. These results leads us to propose a hypothesis that the PI-20 chain feels an extra motional constraint (not identical but somewhat similar to entanglement) even in the iso-ζ state when blended with concentrated PtBS-16 chains, as speculated in the previous work.[18] In the blend with $w_{PtBS} = 20$ wt %, the retardation due to this extra constraint appears to be almost canceled by the acceleration on dilution with the PtBS-16 chains, which possibly results in the observed coincidence of τ_ϵ in this blend and iso-ζ bulk.[40]

At first sight, one may argue that the motional constraint for PI-20 in the iso-ζ state due to PtBS-16 is unreasonable because M_{PtBS} of PtBS-16 is significantly smaller than $M_{e,bulk}^{PtBS}$ for bulk PtBS ($M_{PtBS\text{-}16} \cong 0.4M_{e,bulk}^{PtBS}$). However, this constraint should emerge if the PtBS-16 chains disturb the PI-20 chain to exhibit the free Rouse motion over its bulk entanglement mesh size $a_{bulk\text{-}PI}$ (= 5.1 nm)[21] within its intrinsic time for this motion, τ_e. The τ_e is related to the global Rouse equilibration time for the whole contour of the PI-20 chain, τ_R, as $\tau_e = \{M_{PI}/M_{e,bulk}^{PI}\}^{-2}\tau_R \cong 0.06\tau_R$, and the terminal relaxation time τ_ϵ of the *entangled* PI-20 chain is longer than τ_R; namely, $\tau_e < 0.06\tau_\epsilon$. Thus, the PI-20 chain should feel some constraint from the PtBS-16 chains if its Rouse motion over $a_{bulk\text{-}PI}$ requires a time $>0.06\tau_\epsilon$ in the presence of PtBS-16. We can focus on the motion of the PtBS-16 chains to examine if this constraint actually emerges, as explained below.

In the blends with $w_{PtBS} = 30$ and 50 wt %, the PtBS-16 chains are moderately overlapping with each other and penetrate the random coils of all PI-20 chains therein. Thus, for the PI-20 chain to exhibit the free Rouse motion over the length scale $a_{bulk\text{-}PI}$, the wriggling motion of the PtBS-16 chains over the same length scale should occur within $\tau_e < 0.06\tau_\epsilon$. From the average end-to-end distance of the PtBS-16 chains, $R_{PtBS} = 7.7$ nm (Table 1), the time required for this wriggling motion can be estimated as $\tau^* = \{a_{bulk\text{-}PI}/R_{PtBS}\}^4\tau_{G,PtBS} = 0.19\tau_{G,PtBS}$. This estimate, obtained under an assumption of the Rouse-type dynamics of PtBS-16 chains, should give the correct order of magnitude of τ^* of these low-M chains.

Since the PtBS-16 chains are the slow component in the blends, we may utilize $\tau_{G,B}$ data of the blend as a whole (instead of $\tau_{G,PtBS}$ of those chains) to estimate $\tau^* \cong 0.19\tau_{G,B}$. This τ^* is considerably longer than $0.06\tau_\epsilon$ of PI-20 at all T examined; see Figure 10. This fact strongly suggests that the slow PtBS-16 chains effectively behave, in the time scale of τ_e, as short but immobilized bulky threads somehow constraining the free Rouse motion of the PI-20 chains even in the iso-ζ state. This constraint should retard the global relaxation of PI-20, which possibly results in the difference of the global relaxation times τ_ϵ of PI-20 in the blends and iso-ζ bulk seen in the bottom panel of Figure 11. Although this motional constraint for PI-20 is a natural consequence of the difference of the terminal relaxation times of PtBS-16 and PI-20, it is still a hypothesis. This hypothesis deserves further study.

In relation to the above hypothesis, one may argue that the magnitude of motional constraint for PI-20 due to PtBS-16 may change with T and this change needs to be incorporated in the correction of the raw a_T data made in prior to the WLF-determination of $T_{iso\text{-}PI}$. However, in the entire range of T examined for $w_{PtBS} = 30$ and 50 wt %, τ_e ($\leq 0.06\tau_\epsilon$) of the PI-20 chains was considerably shorter than $\tau^* \cong 0.19\tau_{G,B}$ (cf. Figure 10) and thus the magnitude of motional constraint should be insensitive to T and hardly affect the WLF-determination of $T_{iso\text{-}PI}$. This T-insensitivity is reflected in the $\tau_\epsilon/\tau_{\epsilon,bulk}$ ratio being almost constant ($\cong$2.4) for those blends.

Thus, in the entire range of w_{PtBS} examined (= 20−50 wt %), the PtBS-16 chains give some constraint to the global motion of the PI-20 chains even in the iso-ζ state. We naturally expect a counter effect of PI-20 on the relaxation of PtBS-16 chains. This effect is later examined through comparison of the relaxation times of PtBS-16 in the blends and iso-ζ bulk.

3.4. Dynamic Behavior of PtBS Chains in Blends. Obviously, the viscoelastic modulus G_B^* of the blends is contributed from both of the PI-20 and PtBS-16 chains. Since these chains have different effective T_g's, the G_B^* data (shown in Figures 4 and 5) did not exhibit the thermo-rheological simplicity. However, the modulus G_{PtBS}^* of the PtBS-16 chains in the blends could exhibit this simplicity. In the remaining part of this section, we first evaluate the PI-20 modulus G_{PI}^* in the blends and further the PtBS-16 modulus G_{PtBS}^* ($=G_B^*-G_{PI}^*$). Then, we utilize the G_{PtBS}^* data to examine the thermo-rheological behavior of PtBS-16 chains in the blends and determine the iso-ζ temperature $T_{iso\text{-}PtBS}$ for PtBS-16. Finally, we examine an effect of PI-20 on the relaxation of PtBS-16 chains in the iso-ζ state (at $T_{iso\text{-}PtBS}$). Readers not interested in details of the evaluation of G_{PI}^* and G_{PtBS}^* may skip the following subsection and directly proceed to subsection 3.4.2 where the effect of PI-20 is discussed.

3.4.1. PtBS Modulus in Blends. The modulus G_{PI}^* of the PI-20 chains in the blends, required for evaluation of G_{PtPS}^* ($= G_B^*-G_{PI}^*$) of the PtBS-16 chains, can be obtained from the $G_{PI,bulk}^*(\omega)$ data of bulk PI-20 (Figure 1) if we know a ratio of the viscoelastic relaxation times τ_G of PI-20 in the blends at a given temperature T and bulk system at $T_{r,bulk}$, $\tau_G(T)/\tau_{G,bulk}(T_{r,bulk})$, as well as a ratio of the terminal viscoelastic relaxation intensities I_G in the blends and bulk, $I_G(T)/I_{G,bulk}(T_{r,bulk})$. These ratios are experimentally determined below to evaluate G_{PI}^* and G_{PtBS}^*.

3.4.1.1. Ratio of Viscoelastic Relaxation Times of PI in Blend and Bulk. The PI-20 chains split into the majority and minority components in the PI-20/PtBS-16 blends with w_{PtBS} = 30 and 50 wt % (cf. Figures 8 and 9). For convenience of evaluation of the $\tau_G(T)/\tau_{G,bulk}(T_{r,bulk})$ ratio for each component, we can express this ratio as a product of three ratios,

$$\frac{\tau_{G,j}(T)}{\tau_{G,bulk\text{-}PI}(T_{r,bulk})} = \left\{\frac{\tau_{\varepsilon,bulk\text{-}PI}(T_{r,bulk})}{\tau_{G,bulk\text{-}PI}(T_{r,bulk})}\right\} \times \left\{\frac{\tau_{\varepsilon,j}(T)}{\tau_{\varepsilon,bulk\text{-}PI}(T_{r,bulk})}\right\} \times \left\{\frac{\tau_{G,j}(T)}{\tau_{\varepsilon,j}(T)}\right\} \quad (10)$$

with j = majority and minority. Here, τ_ϵ is the dielectric relaxation time (in the environments and at the temperatures as indicated). The first ratio is known from the data for bulk PI-20; $\tau_{\epsilon,bulk\text{-}PI}(T_{r,bulk})/\tau_{G,bulk\text{-}PI}(T_{r,bulk}) \cong 2$. The second ratio, $\{\tau_{\epsilon,j}(T)/\tau_{\epsilon,bulk\text{-}PI}(T_{r,bulk})\}$, is identical to $1/\lambda_j$ with λ_j being the frequency reduction factors already determined in Figures 8 and 9. Thus, analysis of the third ratio, $\tau_{G,j}(T)/\tau_{\epsilon,j}(T)$, allows us to evaluate the $\tau_G(T)/\tau_{G,bulk}(T_{r,bulk})$ ratio.

For the majority of PI-20, the dielectric and viscoelastic relaxation is affected by PtBS-16 through the three mechanisms explained earlier, antiplasticization, restriction of DTD/CR (compared to bulk PI-20), and motional constraint due to PtBS-16 that occurs even in the iso-ζ state for PI-20. The antiplasticization just enhances the local friction of PI and thus retards the dielectric and viscoelastic relaxation of PI-20 to the same

extent with respect to the relaxation of bulk PI-20. In other words, the antiplasticization has no influence on the $\tau_{G,j}(T)/\tau_{\epsilon,j}(T)$ ratio. Similarly, the motional constraint due to PtBS-16 should equally retard the dielectric and viscoelastic relaxation to give no effect on this ratio (at least in the range of T examined). In contrast, the restriction of DTD/CR retards the viscoelastic relaxation more significantly than the dielectric relaxation because the latter is insensitive to DTD, as explained earlier for eq 7. The retardation due to this restriction has been quantified through eq 7 as $\tau_{G,\mathrm{maj}}(T) = Q^{3.33}\tau_{G,\text{bulk-PI}}(\text{iso-}\zeta)$ and $\tau_{\epsilon,\mathrm{maj}}(T) = Q\tau_{\epsilon,\text{bulk-PI}}(\text{iso-}\zeta)$, where $\tau_{G,\text{bulk-PI}}(\text{iso-}\zeta)$ and $\tau_{\epsilon,\text{bulk-PI}}(\text{iso-}\zeta)$ are the viscoelastic and dielectric relaxation times in the iso-ζ bulk and the factor Q has been determined by eq 9. Thus, we obtain a relationship, $\tau_{G,\mathrm{maj}}(T)/\tau_{\epsilon,\mathrm{maj}}(T) = Q^{2.33}\{\tau_{G,\text{bulk-PI}}(\text{iso-}\zeta)/\tau_{\epsilon,\text{bulk-PI}}(\text{iso-}\zeta)\} = Q^{2.33}\{\tau_{G,\text{bulk-PI}}(T_{\mathrm{r,bulk}})/\tau_{\epsilon,\text{bulk-PI}}(T_{\mathrm{r,bulk}})\}$, where we have considered a fact that the $\tau_{G,\text{bulk-PI}}/\tau_{\epsilon,\text{bulk-PI}}$ ratio ($\cong 1/2$) for bulk PI does not change with T. Utilizing this relationship in eq 10 and considering the coincidence of the second ratio therein and $1/\lambda_{\mathrm{fast}}$, we finally find an expression of the $\tau_{G,\mathrm{maj}}(T)/\tau_{G,\text{bulk-PI}}(T_{\mathrm{r,bulk}})$ ratio,

$$\frac{\tau_{G,\mathrm{maj}}(T)}{\tau_{G,\text{bulk-PI}}(T_{\mathrm{r,bulk}})} = Q^{2.33}/\lambda_{\mathrm{fast}} \tag{11}$$

for the majority of PI-20. Thus, this ratio can be evaluated from the known values of Q (≤ 1.31 at all T examined; cf. eq 9) and λ_{fast} (determined in Figures 8 and 9).

Now, we turn our attention to the minority of PI-20. Equations 7 and 9 were obtained for the fastest component in blends and cannot apply rigorously to the minority (second fastest component). However, the restriction of DTD/CR due to PtBS-16 should be weaker for the minority PI-20 than for the majority PI-20 because the relaxation time difference from PtBS-16 is smaller for the former. Since the retardation due to the restriction of DTD/CR is just moderate even for the majority (as quantified by $Q \leq 1.31$), we may safely approximate that the minority is subjected to negligibly weak retardation to have $\{\tau_{G,\mathrm{min}}(T)/\tau_{\epsilon,\mathrm{min}}(T)\} = \{\tau_{G,\text{bulk-PI}}(T_{\mathrm{r,bulk}})/\tau_{\epsilon,\text{bulk-PI}}(T_{\mathrm{r,bulk}})\}$ in eq 10. (In fact, eqs 7 and 9, if applied to the minority, gave $Q \cong 1$.) Then, eq 10 reduces to

$$\frac{\tau_{G,\mathrm{min}}(T)}{\tau_{G,\text{bulk-PI}}(T_{\mathrm{r,bulk}})} = 1/\lambda_{\mathrm{slow}} \tag{12}$$

for the minority of PI-20. Thus, the $\tau_G(T)/\tau_{G,\text{bulk-PI}}(T_{\mathrm{r,bulk}})$ ratio for the minority PI-20 can be evaluated from the known value of λ_{slow} (determined in Figures 8 and 9).

3.4.1.2. Ratio of Viscoelastic Relaxation Intensities of PI in Blend and Bulk. Since the majority of PI-20 is the fastest component in the PI/PtBS blend, its terminal viscoelastic relaxation intensity $I_{G,\mathrm{maj}}(T)$ should not be affected by the slower relaxation of the minority and PtBS-16, as similar to the situation in PI/PI blends.[33] Then, $I_{G,\mathrm{maj}}(T)$ is simply proportional to T and the volume fraction of the majority, $\phi_{\mathrm{PI}}\upsilon_{\mathrm{fast}}$ (υ_{fast} = majority fraction in the ensemble of PI-20 chains). Thus, a ratio of $I_{G,\mathrm{maj}}(T)$ to the intensity $I_{G,\text{bulk-PI}}(T_{\mathrm{r,bulk}})$ of bulk PI-20 at $T_{\mathrm{r,bulk}}$ (= 303K), is given by

$$\frac{I_{G,\mathrm{maj}}(T)}{I_{G,\text{bulk-PI}}(T_{\mathrm{r,bulk}})} = \frac{1}{b_T'}\phi_{\mathrm{PI}}\upsilon_{\mathrm{fast}} \tag{13}$$

with $b_T' = T_{\mathrm{r,bulk}}/T$ for majority of PI-20.

The change in the density, being much less significant compared to the change of T (in unit of K), has been safely neglected in the expression of b_T' shown in eq 13 as well as in eqs 14 and 15.

We need a little more detailed consideration for the evaluation of $I_{G,\mathrm{min}}(T)$ for the minority of PI-20. If the majority relaxes *much* faster than the minority, the former behaves as a simple solvent for the relaxation of the latter to dilute the entanglement mesh. In fact, this type of dilution and the corresponding decrease of I_G are known for binary blends of chemically identical, high-M and low-M chains with their relaxation times in the blends differing by a factor $\gg 10$.[33,41] However, if their relaxation times differ only by a factor of 10 or less, the low-M chains (fast component) does not behave as the solvent for the high-M chains (slow component) and the terminal relaxation intensity of the latter is proportional to its volume fraction.[41] This should be the case for the minority component of PI-20 in our blends: τ_ϵ is longer for the minority than for the majority by a factor <10, as noted in top two panels of Figure 10. Furthermore, the PtBS-16 chains relaxing slower than the minority never behave as the solvent for the minority. Thus, $I_{G,\mathrm{min}}(T)$ should be proportional to the minority volume fraction, $\phi_{\mathrm{PI}}(1 - \upsilon_{\mathrm{fast}})$. Then, the $I_{G,\mathrm{min}}(T)/I_{G,\text{bulk-PI}}(T_{\mathrm{r,bulk}})$ ratio for the minority of PI-20 is given by

$$\frac{I_{G,\mathrm{min}}(T)}{I_{G,\text{bulk-PI}}(T_{\mathrm{r,bulk}})} = \frac{1}{b_T'}\phi_{\mathrm{PI}}(1 - \upsilon_{\mathrm{fast}}) \tag{14}$$

with $b_T' = T_{\mathrm{r,bulk}}/T$.

Here, a comment needs to be added for the above argument for the viscoelastic relaxation intensity of PI-20 chains. Obviously, the antiplasticization and restriction of DTD/CR due to PtBS-16 have no influence on the intensity. However, the PI-20 chains are motionally constrained by the slow PtBS-16 chains even in the iso-ζ state for PI (cf. discussion for the bottom panel of Figure 11), and this constraint might potentially affect the viscoelastic relaxation intensity of PI-20. Namely, if this constraint is rigorously identical to the usual *entanglement* in bulk homopolymer systems, the $\tau_{\epsilon,\mathrm{blend}}/\tau_{\epsilon,\mathrm{bulk}}$ ratio of $\cong 2.4$ seen for the PI-20 chains in the blends and iso-ζ bulk system is to be interpreted as a result of a decrease of the PI entanglement molecular weight M_e^{PI} on blending with PtBS-16 chains. For this case, we have to consider an increase of the viscoelastic relaxation intensity (or plateau modulus). However, the PtBS-16 chains are too short to form the entanglement network by themselves, as clearly noted from their molecular weight $M_{\mathrm{PtBS}} < M_{\mathrm{e,bulk}}^{\mathrm{PtBS}}$. Thus, the motional constraint for PI-20 due to PtBS-16 does not result from incorporation of the PI-20 chains in an entanglement network denser than that in bulk PI-20 system. Instead, this constraint merely results from the "slowness" of the PtBS-16 motion: In the time scale of the PI-20 relaxation, the PtBS-16 chains just behave as short but immobilized bulky threads to motionally constrain the PI-20 chains. For this case, the constraint should not significantly affect the relaxation intensity of the PI-20 chains, which allows us to utilize eqs 13 and 14.

3.4.1.3. Thermo-Rheological Behavior of PtBS in Blend. On the basis of eqs 11–14, we can express the modulus of PI-20 in the blend at a temperature T, $G_{\mathrm{PI}}^*(\omega,T)$, in terms of the $G_{\mathrm{PI,bulk}}^*(\omega)$ data of bulk PI-20 at T_{r} (= 303K) as[42]

$$G_{\mathrm{PI}}^*(\omega,T) = \frac{\phi_{\mathrm{PI}}}{b_T'}[\upsilon_{\mathrm{fast}}G_{\mathrm{PI,bulk}}^*(Q^{2.33}\omega/\lambda_{\mathrm{fast}}) + \{1 - \upsilon_{\mathrm{fast}}\}G_{\mathrm{PI,bulk}}^*(\omega/\lambda_{\mathrm{slow}})] \tag{15}$$

with $b_T' = T_{\mathrm{r,bulk}}/T$. Since the parameters Q, λ_{fast}, υ_{fast}, and λ_{slow} have been determined through the analysis of the dielectric data, $G_{\mathrm{PI}}^*(\omega,T)$ was evaluated from the $G_{\mathrm{PI,bulk}}^*(\omega)$ data with no ambiguity. Utilizing this $G_{\mathrm{PI}}^*(\omega,T)$, we evaluated the modulus of the PtBS-16 chains in the blends with $w_{\mathrm{PtBS}} = 30$ and 50 wt % as

$$G_{\mathrm{PtBS}}^*(\omega,T) = G_{\mathrm{B}}^*(\omega,T) - G_{\mathrm{PI}}^*(\omega,T) \tag{16}$$

(For the blend with $w_{\mathrm{PtBS}} = 20$ wt %, $G_{\mathrm{B}}^*(\omega,T)$ was very close to $G_{\mathrm{PI}}^*(\omega,T)$ and this subtraction could not be made accurately.[20])

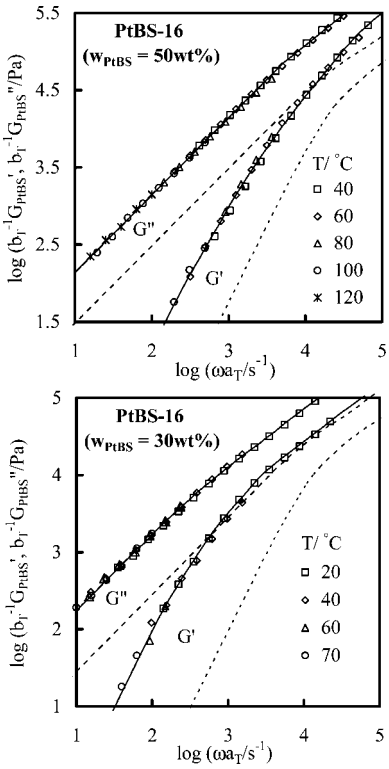

Figure 12. Test of the time−temperature superposability for the $b_T^{-1}G_{PtBS}$* data of the PtBS-16 chains in the PI-20/PtBS-16 blends with w_{PtBS} = 50 and 30 wt %, with $b_T = T/T_r$ being an intensity correction factor. The dotted curves indicate normalized modulus of bulk PtBS-16 at the iso-ζ temperature, $T_{iso\text{-}PtBS}$. The solid curves are guide for eye. For further details, see text.

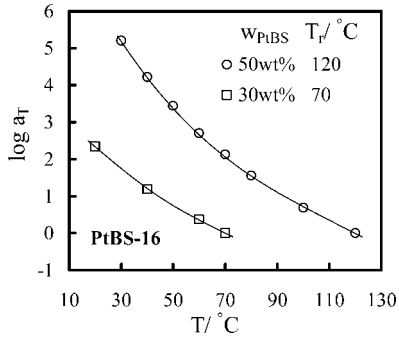

Figure 13. Plots of the time−temperature shift factor a_T for G_{PtBS}*data (shown in Figure 12) against the temperature T.

Figure 12 shows mater curves of the G_{PtBS}*(ω,T) data for w_{PtBS} = 30 and 50 wt % together with shifted modulus of bulk PtBS-16 (dotted curves) explained later. The solid curves are guide for eye. The G_{PtBS}*(ω,T) data at respective T are reduced by an intensity correction factor, $b_T = T/T_r$ (with T and T_r in K unit), and shifted along the ω axis by a factor of a_T to achieve the best superposition with the data at the reference temperature T_r (=70 and 120 °C for w_{PtBS} = 30 and 50 wt %, respectively). The a_T data with respect to these T_r are shown in Figure 13.

As noted in Figure 12, the time−temperature superposition works well for the $b_T^{-1}G_{PtBS}$*(ω,T) data for the blends with w_{PtBS} = 30 and 50 wt %. Thus, the frictional nonuniformity due to the dynamic heterogeneity appears to be erased by the PI-20 chains (relaxing faster than PtBS-16 chains) thereby allowing all PtBS chains to feel the same frictional environment in their terminal relaxation, which confirms the molecular scenario discussed in the previous work.[18]

3.4.1.4. Comment for the Modulus Additivity in PI-20/PtBS-16 Blends. For bulk homopolymers, Inoue and coworkers[37−39] related the glassy and rubbery components of the viscoelastic modulus (or stress) to the torsion around the chain backbone and the axial orientation of the Rouse segments, respectively, and proposed additivity of these modulus components. The additivity of the glassy and rubbery moduli has been a subject of controversy,[43−46] although the stress-optical coefficient data obtained on the basis of this additivity are consistent with the molecular calculation[47] and the nonlinear rheo-optical behavior of glassy polymers is well explained from this additivity.[48]

As for the blends examined in this study, eq 15 is based on the modulus additivity for the majority and minority of the PI-20 chains and eq 16 is based on the modulus additivity for the PI-20 and PtBS-16 chains. One might suspect the validity of eqs 15 and 16 in relation to the controversy explained above. However, it should be emphasized that eqs 15 and 16 represent the additivity of the *rubbery* moduli of those chains. This additivity is well established on the basis of the assignment of the rubbery stress to the orientation of the Rouse segments (as confirmed experimentally from the stress-optical rule for polymeric liquids at high T).[49] Thus, there is no ambiguity in the validity of eqs 15 and 16.

3.4.2. Detailed Dynamics of PtBS in Iso-Frictional State. 3.4.2.1. Iso-ζ Temperature for PtBS in Blend. The relaxation of PtBS-16 in the blends is affected by PI-20 possibly through several different mechanisms. First of all, PtBS-16 is strongly plasticized by PI-20 and the local friction ζ_{PtBS} of the PtBS-16 chains is largely reduced compared to that in the bulk PtBS-16 system at the same T; cf. Figure 3. In addition, the PtBS-16 chains may be subjected to some (topological) constraint from the PI-20 chains; this constraint is a natural counter action of the motional constraint for PI-20 chains due to PtBS-16 discussed for the bottom panel of Figure 11. The shift factor a_T for PtBS-16 (Figure 13) could, in principle, reflect the plasticization effect as well as the constraint from the PI-20 chains. However, the magnitude of the constraint from the PI-20 chains appeared to hardly change with T, as explained/discussed later in more detail. Thus, we may safely consider that the T dependence of a_T for PtBS-16 is equivalent to the T dependence of ζ_{PtBS} ($a_T = \zeta_{PtBS}(T)/\zeta_{PtBS}(T_r)$) to conduct the WLF analysis for the raw a_T data of PtBS (Figure 13) with the method described in Appendix B.

For the PtBS-16 chains in the blends, the iso-ζ temperature $T_{iso\text{-}PtBS}$ corresponding to the reference temperature of bulk PtBS-16, $T_{r,bulk}$ (=$T_{iso\text{-}PtBS}$(bulk)), was obtained from this WLF analysis. The results are summarized in Table 2. The shift factor $a_{T\text{-}iso}$ for PtBS-16 in the blends re-evaluated with respect to $T_{iso\text{-}PtBS}$ is plotted against $T - T_{iso\text{-}PtBS}$ in the top panel of Figure 14. The solid curve indicates WLF eq 2 that describes the a_T data for bulk PtBS-16 with $T_{r,bulk}$ = 171 °C. The plots excellently agree with this solid curve, confirming that $T_{iso\text{-}PtBS}$ was successfully evaluated for PtBS-16 in the blends.

From this agreement, the difference of the iso-ζ temperatures in the blends and bulk, $\Delta T_{iso} = T_{iso\text{-}PtBS}$(blend)$-T_{iso\text{-}PtBS}$(bulk), can be safely regarded as a difference of the effective glass transition temperatures for PtBS-16 in these systems. We may utilize this ΔT_{iso} to estimate the effective T_g of PtBS-16 in the blends as $T_{g,blend}^{PtBS} = T_{g,bulk}^{PtBS} + \Delta T_{iso}$ (with $T_{g,bulk}^{PtBS}$ = 138 °C). These estimates, shown in Figure 3 with thick dotted arrows attached to the DSC traces, are well located at the high-T side of the broad glass transition zone, lending support to our WLF-determination of $T_{iso\text{-}PtBS}$.

3.4.2.2. Relaxation Time of PtBS in Iso-ζ State. The terminal viscoelastic relaxation time of the PtBS-16 chains, $\tau_{G,PtBS} = [G_{PtBS}'/\omega G_{PtBS}'']_{\omega\to 0}$, has been plotted against T in Figure 10

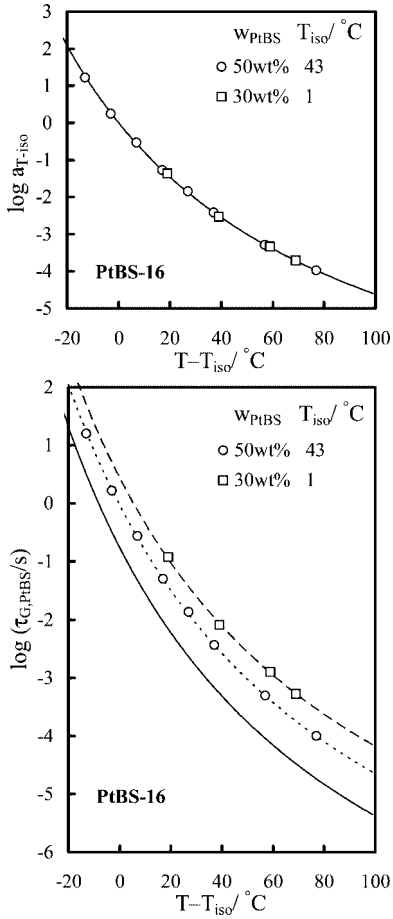

Figure 14. Top panel: Plots of a shift factor $a_{T\text{-iso}}$ of PtBS-16 in the PI-20/PtBS-16 blends with $w_{PtBS} = 50$ and 30 wt % against a distance from the iso-ζ temperature, $T - T_{iso\text{-}PtBS}$. The iso-ζ state for PtBS-16 in the blends is defined with respect to bulk PtBS-16 at 171 °C. The solid curve indicates a_T of bulk PtBS-16 plotted against $T - T_{r,bulk}$ with $T_{r,bulk} = 171$ °C (WLF eq 2). Bottom panel: Viscoelastic relaxation time $\tau_{G,PtBS}$ of PtBS-16 in the blends with $w_{PtBS} = 30$ and 50 wt %. These $\tau_{G,PtBS}$ data are plotted against $T - T_{iso\text{-}PtBS}$. The solid curve indicates $\tau_{G,PtBS}$ of bulk PtBS-16 plotted against $T - T_{r,bulk}$ ($T_{r,bulk} =$ 171 °C). The dotted and dashed curves, respectively, show the bulk $\tau_{G,PtBS}$ data multiplied by factors of 5.4 and 15.8.

(filled squares). We here compare $\tau_{G,PtBS}$ in the blends and bulk in the iso-ζ state. For this purpose, the $\tau_{G,PtBS}$ data for the blends ($w_{PtBS} = 30$ and 50 wt %) are plotted against $T - T_{iso\text{-}PtBS}$ in the bottom panel of Figure 14. The solid curve indicates the $\tau_{G,PtBS}$ data of bulk PtBS-16 plotted against $T - T_{r,bulk}$ ($= T - T_{iso\text{-}PtBS}$), and the dotted and dashed curves show the bulk $\tau_{G,PtBS}$ data multiplied by factors of 5.4 and 15.8, respectively. Clearly, $\tau_{G,PtBS}$ is significantly larger in the blends than in the bulk PtBS system.

This difference of $\tau_{G,PtBS}$ can be noted also for the G_{PtBS}* data. The modulus data of bulk PtBS-16 at $T_{r,bulk} = 444$ K (= 171 °C; cf. Figure 2) were multiplied by the PtBS-16 volume fraction in the blends ($\phi_{PtBS} = 0.47$ and 0.27 for $w_{PtBS} = 50$ and 30 wt %) and reduced by the intensity correction factor, $b_T^\circ = T_{r,bulk}/T_r$ with T_r being the reference temperatures of the blends utilized in Figure 12 ($T_r = 393$ and 343 K for $w_{PtBS} =$ 50 and 30 wt %). As judged from the $T_{iso\text{-}PtBS}$ data in Table 2, the bulk PtBS-16 chains at 248 and 240 °C are iso-frictional with respect to the PtBS-16 chains in the blends at these T_r. The modulus data of bulk PtBS-16 thus corrected, $b_T^{\circ -1}\phi_{PtBS}G_{PtBS,bulk}$*, were shifted from $T_{r,bulk}$ to 248 and 240 °C with the aid of eq 2. This shifted iso-ζ modulus is shown in Figure 12 with the dotted curves. Clearly, the PtBS-16 relaxation in the blends is considerably slower than that shown by these curves.

As demonstrated above, the relaxation of the PtBS-16 chains in the blends is retarded, compared to that in the iso-ζ bulk, by the coexisting PI-20 chains. This fact leads us to propose a hypothesis that the PI-20 chains topologically constrain the PtBS-16 chains thereby retarding the terminal relaxation of PtBS-16. (The constraint for PtBS-16 due to PI-20 seems to be a natural counter action of the constraint for PI-20 due to PtBS-16 discussed earlier). This hypothesis is further discussed below in relation to the entanglement criterion in homopolymer systems.

3.4.2.3. Topological Constraint for PtBS Due to PI. For homopolymers, the criterion of entanglement can be characterized by the number P_e of entanglement strands within a volume a^3, where a is the entanglement mesh size (or tube diameter). This P_e is nearly constant for a variety of flexible homopolymers including PI and PtBS:[21]

$$P_e \equiv \frac{a^3}{V_e} = \frac{a}{p} = 20 \pm 3 \tag{17}$$

In eq 17, V_e represents the occupied volume of the entanglement strand; $V_e = M_e/(\rho N_A)$ with ρ and N_A being the polymer density and Avogadro constant. p is the packing length[21,23,24] defined as a ratio of the occupied volume of the Kuhn segment v_0 to square of the Kuhn length b:

$$p \equiv \frac{v_0}{b^2} \tag{18}$$

Assuming that the criterion for the entanglement, eq 17, holds also for our PI-20/PtBS-16 blends, we examine if the PtBS-16 chains can be topologically constrained by the PI-20 backbone. For this purpose, we estimate an effective packing length in the blends as

$$p_{blend} = n_{PtBS}p_{PtBS} + n_{PI}p_{PI} \tag{19}$$

In eq 19, n_{PtBS} and n_{PI} ($=1 - n_{PtBS}$) denote the number fractions of the Kuhn segments of PtBS and PI in the blends, and p_{PtBS} ($=0.48_1$ nm)[21] and p_{PI} ($=0.26_9$ nm)[21] represent the intrinsic packing lengths of the PtBS and PI chains, respectively. Since the molecular weight of the Kuhn segment M_K is considerably larger for PtBS ($M_{K,PtBS} \cong 1500$)[50] than for PI ($M_{K,PI} \cong 130$),[21] $n_{PtBS} \ll n_{PI}$ in the PI-20/PtBS-16 blends and p_{blend} was close to p_{PI}; $n_{PtBS} = 0.036$ and 0.080 and $p_{blend} = 0.27_7$ and 0.28_6 nm for the blends with $w_{PtBS} = 30$ and 50 wt %, respectively. Correspondingly, the effective entanglement mesh size in the blend estimated from eq 17, $a_{blend} \cong 20p_{blend}$ (=5.5 and 5.7 nm for $w_{PtBS} = 30$ and 50 wt %), is not very different from a_{PI} (= 5.1 nm)[21] for bulk PI.

These a_{blend} values are smaller than the average end-to-end distance of PtBS-16 chains, $R_{PtBS} = 7.7$ nm (cf. Table 1), lending qualitative support to our hypothesis that the PI-20 chains topologically constrain the PtBS-16 chains to retard the terminal relaxation of PtBS-16: The average volume fraction of the PI-20 segments in a random coil of each PtBS-16 chain in the blends is considerably large ($\phi_{PI} = 0.53$ and 0.73 for $w_{PtBS} =$ 50 and 30 wt %), and the PI backbone is much more flexible compared to the PtBS backbone. Thus, each random coil of PtBS seems to acquire a longer contour of chain backbone in it when blended with PI-20, which may result in the topological constraint for the PtBS-16 chains (somewhat similar to the usual entanglement). Although the difference between a_{blend} and R_{PtBS} is not very large, moderate overlapping of neighboring PtBS chains characterized by the C_{PtBS}/C_{PtBS}* ratio (= 1.4 and 2.3 for $w_{PtBS} = 30$ and 50 wt %; cf. Table 2) may enhance this constraint to significantly retard the

terminal relaxation of PtBS-16 in the iso-ζ state (by a factor >5; cf. bottom panel of Figure 14).

The above molecular picture is still a hypothesis and a further study is desired. At the same time, it should be emphasized that the analysis based on the concept of the packing length is not contradicting to this hypothesis but rather suggests a general possibility of enhancement of the topological constraint for bulky chains on blending with flexible chains.

3.4.2.4. Hypothesis for PtBS-16 Relaxation Mechanism. The PtBS-16 chains relax more slowly in the blends than in the iso-ζ bulk and this difference is quite possibly due to the topological constraint from the PI-20 chains, as explained above. This result suggests that the motion of the PI-20 chains triggers the terminal relaxation of PtBS-16 chains in the blends. This relaxation mechanism is similar, *in a sense that the relaxation of a focused chain (probe) is governed by the surrounding chains (matrix)*, to the constraint release (CR)[28,49,51,52] mechanism in homopolymer blends. However, we also note an important difference: In homopolymer blends, the CR relaxation of the probe chain is activated by the global motion of the matrix chains and thus the CR relaxation time of the probe is essentially proportional to the matrix relaxation time, as expected theoretically[49,51,52] and confirmed experimentally.[28] This proportionality emerges because the probe exhibits the local CR jump over the entanglement mesh size a immediately after the global motion of the matrix chain occurs, i.e., the probe has the local CR-jump time close to the matrix relaxation time. These conditions are *not* satisfied for the PtBS-16 chains in the blends: As seen in Figure 10, the relaxation time of PtBS-16 (probe), $\tau_{G,\mathrm{PtBS}}$, is not at all proportional to the relaxation time of PI-20 (matrix), τ_ϵ. Furthermore, *if* the PtBS-16 chains relax through the usual Rouse-CR mechanism, their local CR-jump time for the length scale of a_{blend} ($\cong$ "0.7" R_{PtBS} as discussed earlier) is given by $\tau^{**} \cong \{a_{\mathrm{blend}}/R_{\mathrm{PtBS}}\}^4 \tau_{G,\mathrm{PtBS}} \cong 0.2\tau_{G,\mathrm{PtBS}}$. This τ^{**} is much longer than τ_ϵ of PI-20 in particular at low T; cf. Figure 10.

Considering the above results, we propose a hypothesis that a focused PtBS-16 chain (probe) in the blends with $C_{\mathrm{PtBS}} > C_{\mathrm{PtBS}}^*$ relaxes when the constraint from the overlapping PtBS-16 chains (matrix) is released through the matrix motion. This constraint for the probe in turn emerges because a flexible PI-20 chain simultaneously penetrates the random coils of the probe and matrix PtBS-16 chains. In other words, the PI-20 chains seem to just create the topological constraint for the PtBS-16 chains by stitching the random coils of the PtBS-16 chains, and the rate-determining step for release of this constraint is the motion of the PtBS-16 chains themselves (not the motion of the PI-20 chains). This relaxation mechanism of PtBS-16 is considerably different from the usual CR mechanism but hereafter named as *pseudo-CR* just for convenience of discussion.

The local pseudo-CR jump frequency in the iso-ζ state would decrease and thus the terminal relaxation time $\tau_{G,\mathrm{PtBS}}$ of PtBS-16 would increase with increasing volume fraction ϕ_{PI} of the stitching PI-20 chains in the PtBS-16 random coil. Since ϕ_{PI} is larger for smaller w_{PtBS} ($\phi_{\mathrm{PI}} = 0.73$ and 0.53 for $w_{\mathrm{PtBS}} = 30$ and 50 wt %), we expect that a difference of $\tau_{G,\mathrm{PtBS}}$ in the blend and iso-ζ bulk is larger for smaller w_{PtBS}. This expectation is in harmony with the observation ($\tau_{G,\mathrm{PtBS}}$ is larger for $w_{\mathrm{PtBS}} = 30$ wt % than for $w_{\mathrm{PtBS}} = 50$ wt %; cf. Figure 14).

If the PtBS-16 chains relax through the pseudo-CR mechanism, the T dependence of the shift factor a_{T} for PtBS-16 would not be affected by the motion of the PI-20 chains because the PI-20 chains stitch the PtBS-16 random coils to the same extent irrespective of T. Then, the raw a_{T} data of the PtBS-16 chains just reflect the change of their local friction with T, i.e., $a_{\mathrm{T}} = \zeta_{\mathrm{PtBS}}(T)/\zeta_{\mathrm{PtBS}}(T_{\mathrm{r}})$, which is consistent with the $T_{\mathrm{iso\text{-}PtBS}}$ determination through the WLF analysis for the raw a_{T} data (cf. Figure 14).

The pseudo-CR mechanism for the PtBS-16 relaxation is qualitatively consistent with the observation, as explained above. However, this mechanism has not been confirmed from separate experiments and is still hypothetical. Further study is desired for this problem.

4. Concluding Remarks

The viscoelastic and dielectric behavior was examined for statistically homogeneous PI-20/PtBS-16 blends with $w_{\mathrm{PtBS}} =$ 50% and 30% at several different temperatures ($\leq$120 °C). PI-20 (with $M_{\mathrm{PI}} \cong 4M_{\mathrm{e,bulk}}^{\mathrm{PI}}$) was moderately entangled while PtBS-16 (with $M_{\mathrm{PtBS}} \cong 0.4M_{\mathrm{e,bulk}}^{\mathrm{PtBS}}$) was not entangled in respective bulk systems. The dielectric relaxation of these blends exclusively reflected the global motion of the PI-20 chains while the viscoelastic relaxation was contributed from the motion of both of the PI-20 and PtBS-16 chains. Comparison of the dielectric and viscoelastic data indicated that the PI-20 chains relaxed faster than the PtBS-16 chains in the blends at the temperatures examined.

The failure of the time−temperature superposition observed for the dielectric data was related to the nonuniform frictional environment for PI-20 due to the slow PtBS-16 chains that was effectively quenched over a length scale of R_{PI} in the time scale of the global relaxation of the PI-20 chains. The dielectric spectra indicated that the PI-20 chains in the blends were split into the majority and minority components, the former feeling a smaller friction and relaxing faster compared to the latter. The difference of the relaxation rates of these components decreased and the majority fraction increased with increasing temperature, thereby resulting in the failure of the time−temperature superposition. (The dielectric spectra of the blends approached the spectrum of bulk PI-20 at sufficiently high temperatures.)

In contrast, the superposition was valid for the terminal relaxation of the PtBS-16 chains. In this time scale, the faster PI-20 chains appeared to have erased the dynamic heterogeneity to allow the PtBS-16 chains to relax in a uniform frictional environment and obey the superposition.

Detailed analysis of the relaxation times of PI-20 and PtBS-16 chains in the blends suggested that both of these chains relaxed slower in the blends than in respective *iso-frictional* (iso-ζ) bulk systems. The PtBS-16 chains were less mobile than the PI-20 chains. Thus, the PtBS-16 chains appeared to behave as short and bulky threads that are effectively immobilized in the time scale of PI-20 relaxation. These immobilized threads penetrate the random coil of the PI-20 chain to retard the PI-20 relaxation. This retardation is certainly possible even through PtBS-16 had low M_{PtBS} ($\cong 0.4M_{\mathrm{e,bulk}}^{\mathrm{PtBS}}$). In contrast, the faster PI-20 chains cannot retard the PtBS-16 relaxation in the same way. However, analysis on the basis of the concept of packing length suggested that the PI-20 chain, being much more flexible than the PtBS-16 chain, enlarged the total chain backbone length in the PtBS-16 random coil above a critical value for the topological constraint (being somewhat similar, but not identical, to the usual entanglement of bulk homopolymers). This constraint possibly retarded the PtBS-16 relaxation in the blends compared to the iso-ζ bulk.

Acknowledgment. We thank Professor Hironori Kaji for his generous help for the DSC measurement and Ms. Eri Mishima and Professor Shigeru Yamago for their generous help for the NMR measurement. This work was partly supported by Grant-in-Aid for Scientific Research on Priority Area "Soft Matter Physics" from the Ministry of Education, Culture, Sports, Science and Technology (Grant No. 18068009).

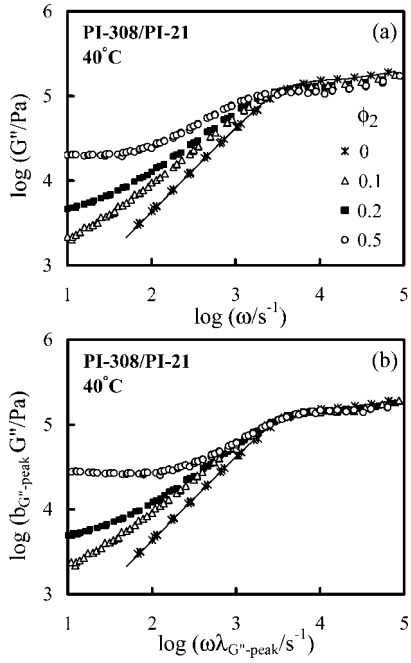

Figure 15. Top panel: Angular frequency dependence of the loss modulus, G'', obtained for a series of PI/PI binary blends with the component molecular weights of $M_1 = 21.4 \times 10^3$ and $M_2 = 30.8 \times 10^4$. The data were taken from ref 33. Bottom panel: Superposition of the G'' curves shown in the top panel.

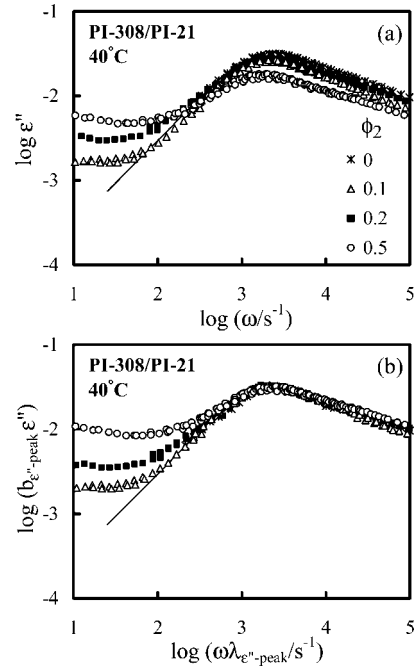

Figure 16. Top panel: Angular frequency dependence of the dielectric loss, ϵ'', obtained for a series of PI/PI binary blends with the component molecular weights of $M_1 = 21.4 \times 10^3$ and $M_2 = 30.8 \times 10^4$. The data were taken from ref 33. Bottom panel: Superposition of the ϵ'' curves shown in the top panel.

Appendix A. Retardation of Relaxation Due To Restriction of DTD/CR

Within the current molecular model (tube model) for the entanglement dynamics of linear homopolymers,[28,49,51,52] we may consider that the moderately entangled bulk PI-20 chains relax through reptation, contour length fluctuation, and dynamic tube dilation (DTD)/constraint release (CR). The DTD/CR contribution to the relaxation is restricted when the PI-20 chains are blended with slower chains. This is the case for the PI-20 chains in the PI-20/PtBS-16 blends. However, the PI-20 relaxation in those blends should be also affected by the other mechanisms, the antiplasticization and extra motional constraint due to the bulky PtBS-16 chains. The viscoelastic and dielectric data obtained for binary blends of low-M and high-M PI chains[33,53] are free from these mechanisms and thus helpful for quantifying the effect of the restriction of DTD/CR on the PI-20 relaxation. This Appendix organizes these data in a form of empirical equations.

For PI/PI binary blends with the component molecular weights $M_1 = 21.4 \times 10^3$ (PI-21; component-1) and $M_2 = 30.8 \times 10^4$ (PI-308; component-2), the angular frequency (ω) dependencies of the viscoelastic and dielectric losses,[33] G'' and ϵ'', are shown in the top panels of Figures 15 and 16, respectively. The data are shown for monodisperse PI-21 and the blends with the PI-308 volume fraction $\phi_2 \geq 0.1$. (For clarity of Figure, the data for smaller ϕ_2 are not shown.) The molecular weight of PI-21 is close to that of PI-20 utilized in this study. The relaxation seen in those panels is the terminal relaxation of PI-21, and the upturn noted at the low ω side of the panels reflects the relaxation of PI-308 (high-M component) occurring at $\omega < 10\ s^{-1}$. We note that peaks of G'' and ϵ'' shift to lower ω and thus both of the viscoelastic and dielectric relaxation processes of PI-21 are retarded with increasing ϕ_2 (≥ 0.1). The DTD/CR mechanism working in the monodisperse PI-21 system is restricted by the slower/longer PI-308 chains to give this retardation. In relation to this point, we note that the peak shift is more significant for G'' than for ϵ''. Namely, the restriction of DTD/CR gives a smaller effect for the dielectric relaxation than for the viscoelastic relaxation. This difference emerges because the terminal dielectric relaxation of the PI chain reflects a decay of the orientational memory of its end-to-end vector while the viscoelastic relaxation detects a decay of the isochronal orientational anisotropy of the Rouse segments: The orientational memory hardly decays but the isochronal anisotropy decays significantly on dilation of the tube that confines the chain.[28,33]

The magnitude of this retardation due to restriction of DTD/CR, represented as the ratios of the viscoelastic and dielectric relaxation times of PI-21 in the blends to those in monodisperse PI-21 system, $\tau_{G1}(\phi_2)/\tau_{G1}(0)$ and $\tau_{\epsilon 1}(\phi_2)/\tau_{\epsilon 1}(0)$, can be evaluated by superposing the G'' and ϵ'' curves of the blends on those of the monodisperse PI-21 system. For this purpose, we multiplied the G'' and ϵ'' data of the blends by intensity correction factors b and shifted these data along the ω axis by factors λ to achieve the best superposition; see the bottom panels of Figures 15 and 16. (The b factor was close to the volume fraction of PI-21.) The viscoelastic $\tau_{G1}(\phi_2)/\tau_{G1}(0)$ ratio, identical to the horizontal shift factor for the G'' curves, is plotted against ϕ_2 in Figure 17; see unfilled circles. For clarity of the plots, the dielectric $\tau_{\epsilon 1}(\phi_2)/\tau_{\epsilon 1}(0)$ ratio is not shown in Figure 17. Instead, this ratio is plotted against the viscoelastic ratio in Figure 18 (cf. circles).

For PI-308/PI-94 binary blends[53] having a higher M_1 ($=94.0 \times 10^3$; PI-94) compared to the PI-308/PI-21 blends, we similarly evaluated the $\tau_{G1}(\phi_2)/\tau_{G1}(0)$ and $\tau_{\epsilon 1}(\phi_2)/\tau_{\epsilon 1}(0)$ ratios. These ratios are shown in Figures 17 and 18 with unfilled triangles. We also evaluated the $\tau_{G1}(\phi_2)/\tau_{G1}(0)$ ratio for two series of binary blends of polystyrenes[41] (PS) having ($10^{-4}M_1$, $10^{-4}M_2$) = (3.63, 29.4) and (16.1, 29.4) and ϕ_2 in a range between 0.03 and 0.6. The results are shown in Figure 17 with unfilled diamonds and squares. (No dielectric $\tau_{\epsilon 1}(\phi_2)/\tau_{\epsilon 1}(0)$ ratio is available for PS/PS blends because PS chains have no type-A dipole.)

As seen in Figure 18, the $\tau_{G1}(\phi_2)/\tau_{G1}(0)$ and $\tau_{\epsilon 1}(\phi_2)/\tau_{\epsilon 1}(0)$ ratios for the PI/PI blends are well correlated with each other because both ratios represent the effect of the restriction of DTD/CR on the relaxation of the fast component. A rigorous molecular theory of DTD/CR, if available, would enable us to

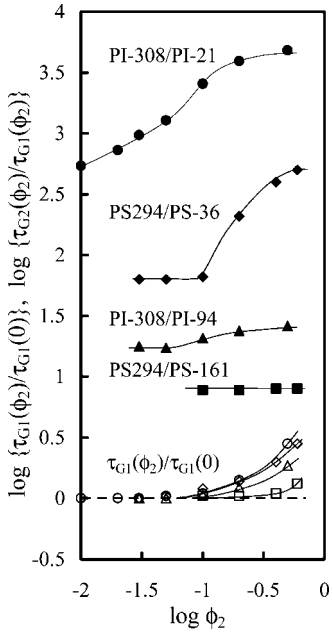

Figure 17. Viscoelastic relaxation time ratios of fast component in blend and monodisperse bulk state, $\tau_{G1}(\phi_2)/\tau_{G1}(0)$ (unfilled symbols), and those of the slow and fast components in the same blend, $\tau_{G2}(\phi_2)/\tau_{G1}(\phi_2)$ (filled symbols). These ratios are plotted against volume fraction of the slow component, ϕ_2. The data were taken from ref 33 (for PI-308/PI-21), ref 53 (for PI-308/PI-94), and ref 41 (for PS/PS).

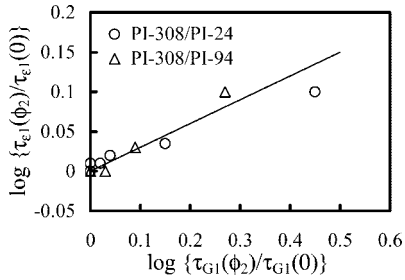

Figure 18. Relationship between the $\tau_{\epsilon 1}(\phi_2)/\tau_{\epsilon 1}(0)$ and $\tau_{G1}(\phi_2)/\tau_{G1}(0)$ ratios for PI-308/PI-21 and PI-308/PI-94 blends. These ratios represent magnitudes of the retardation of the dielectric and viscoelastic relaxation of the fast component in these blends on restriction of DTD/CR. (This retardation is defined with respect to the monodisperse system of the fast component). The solid line indicates the empirical eq A1. The data were taken from refs 33 and 53.

accurately describe this correlation. However, no such theory is available at this moment. Thus, we here adopt an empirical approach by utilizing an empirical equation (solid line in Figure 18) that satisfactorily describes the plots shown therein,

$$Q \equiv \left(\frac{\tau_{\varepsilon 1}(\phi_2)}{\tau_{\varepsilon 1}(0)}\right) = \left(\frac{\tau_{G1}(\phi_2)}{\tau_{G1}(0)}\right)^{0.3} \qquad \text{(A1)}$$

Note that a relationship $\tau_{\epsilon 1}(\phi_2)/\tau_{\epsilon 1}(0) < \tau_{G1}(\phi_2)/\tau_{G1}(0)$ holds (cf. Figure 18) because the dielectric relaxation is not sensitive to DTD compared to the viscoelastic relaxation. The empirical exponent of 0.3 (<1) appearing in eq A1 is a consequence of this relationship.

The viscoelastic $\tau_{G1}(\phi_2)/\tau_{G1}(0)$ ratio increases with increasing M_2/M_1 ratio and with increasing ϕ_2, as noted in Figure 17. This tendency reflects an obvious fact that the restriction of DTD/CR for the component 1 becomes less significant when the component molecular weights M_1 and M_2 become closer to each other and/or the high-M component 2 becomes dilute. (In an extreme cases of $M_2 \to M_1$ or $\phi_2 \to 0$, the blend reduces to the monodisperse system of the component 1 and the restriction of DTD/CR defined *with respect to this system* vanishes.) Thus, the M_2/M_1 ratio and ϕ_2 can be utilized as the empirical parameters that determine the $\tau_{G1}(\phi_2)/\tau_{G1}(0)$ ratio, i.e., the parameters determining the magnitude of the retardation of the fast component relaxation due to the restriction of DTD/CR. However, for the PI-20/PtBS-16 blends examined in this paper, the M_2/M_1 ratio and ϕ_2 cannot be conveniently utilized as such parameters because the PI-20 and PtBS-16 chains therein have different local frictions that change with T differently. Thus, we have to find the other parameter(s) that is experimentally measurable and can properly specify the $\tau_{G1}(\phi_2)/\tau_{G1}(0)$ ratio for PI-20 (fast component in the PI-20/PtBS-16 blends).

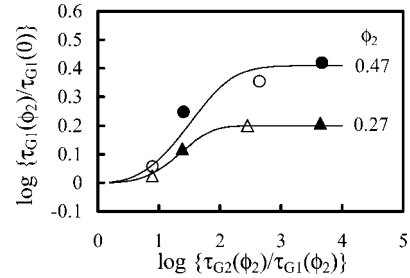

Figure 19. Relationship between the $\tau_{G1}(\phi_2)/\tau_{G1}(0)$ and $\tau_{G2}(\phi_2)/\tau_{G1}(\phi_2)$ ratios for the blends with $\phi_2 = 0.27$ and 0.47. The plots were made by interpolating the data points in Figure 17. The $\tau_{G1}(\phi_2)/\tau_{G1}(0)$ ratio represents the magnitude of the retardation of the viscoelastic relaxation of the fast component in the blends due to restriction of DTD/CR, and the $\tau_{G2}(\phi_2)/\tau_{G1}(\phi_2)$ ratio specifies a difference of the relaxation times of the fast and slow components. The solid curves indicate the empirical eq A2.

For this purpose, we can focus on a ratio the viscoelastic relaxation times of the fast and slow components in the same blend, $\tau_{G2}(\phi_2)/\tau_{G1}(\phi_2)$. This ratio does not uniquely determine the $\tau_{G1}(\phi_2)/\tau_{G1}(0)$ ratio when ϕ_2 is varied. (Irrespective of the $\tau_{G2}(\phi_2)/\tau_{G1}(\phi_2)$ value, $\tau_{G1}(\phi_2)/\tau_{G1}(0) \to 1$ as $\phi_2 \to 0$.) Nevertheless, for a given ϕ_2 value, we expect that the $\tau_{G2}(\phi_2)/\tau_{G1}(\phi_2)$ ratio can be conveniently utilized as the empirical parameter determining the $\tau_{G1}(\phi_2)/\tau_{G1}(0)$ ratio.

In Figure 17, the $\tau_{G2}(\phi_2)/\tau_{G1}(\phi_2)$ data obtained for respective PI/PI and PS/PS blends are shown with the filled symbols. Interpolating these data as well as the $\tau_{G1}(\phi_2)/\tau_{G1}(0)$ data (unfilled symbols), we evaluated the $\tau_{G2}(\phi_2)/\tau_{G1}(\phi_2)$ and $\tau_{G1}(\phi_2)/\tau_{G1}(0)$ values for given values of $\phi_2 = 0.27$ and 0.47 (corresponding to $w_{PtBS} = 30$ and 50 wt % in our PI-20/PtBS-16 blends). Figure 19 shows a relationship between the $\tau_{G1}(\phi_2)/\tau_{G1}(0)$ and $\tau_{G2}(\phi_2)/\tau_{G1}(\phi_2)$ ratios thus evaluated. The filled and unfilled symbols indicate the plots obtained from the data for the PI/PI and PS/PS blends, respectively. The plots obtained from different blends are smoothly connected, suggesting that the $\tau_{G2}(\phi_2)/\tau_{G1}(\phi_2)$ ratio indeed works as the empirical parameter specifying the $\tau_{G1}(\phi_2)/\tau_{G1}(0)$ ratio for given ϕ_2.

We also note that the $\tau_{G1}(\phi_2)/\tau_{G1}(0)$ ratio tends to become constant for large $\tau_{G2}(\phi_2)/\tau_{G1}(\phi_2)$ values. This tendency naturally emerges because DTD/CR is fully restricted to a level determined by ϕ_2 once the $\tau_{G2}(\phi_2)/\tau_{G1}(\phi_2)$ ratio is increased to a certain critical value and a further increase of this ratio results in no change of the magnitude of restriction. The solid curves in Figure 19 show an empirical equation mimicking this tendency (identical to eq 6 in the text),

$$\log\left(\frac{\tau_{G1}(\phi_2)}{\tau_{G1}(0)}\right) = B \tanh\left\{\alpha\left[\log\left(\frac{\tau_{G2}(\phi_2)}{\tau_{G1}(\phi_2)}\right)\right]^q\right\} \qquad \text{(A2)}$$

The coefficients (B, α, q) are (0.2, 0.23, 3) and (0.41, 0.2, 2.5) for $\phi_2 = 0.27$ and 0.47, respectively. For our PI-20/PtBS-16 blends, we combined eq A2 with a harmless approximation ($\tau_{G2}(\phi_2)$ of PtBS-16 being replaced by the directly measurable

$\tau_{GB}(\phi_2)$ of the blend as a whole) to estimate the $\tau_{G1}(\phi_2)/\tau_{G1}(0)$ ratio for PI-20.

Appendix B. WLF Analysis (Iso-ζ Correction)[22]

The WLF-type shift factor a_T, defined with respect to an arbitrarily chosen reference temperature T_r, exhibits the temperature dependence given by

$$\log a_T = -\frac{C_1(T-T_r)}{C_2+(T-T_r)} \quad \text{(B1)}$$

C_1 and C_2 are the WLF coefficients that are related, within the free volume model, to the fractional free volume $f(T_r)$ at T_r and the thermal expansion coefficient of free volume α_f as $C_1 = 0.4343/f(T_r)$ and $C_2 = f(T_r)/\alpha_f$.[22] These coefficients can be determined from plots of $(\log a_T)^{-1}$ data against $(T - T_r)^{-1}$: The plots give a straight line with a slope of $-C_2/C_1$ and an intercept of $-1/C_1$ (as long as a_T obeys the WLF eq B1). From these C_1 and C_2 data, we can determine the values of $f(T_r)$ and α_f. Then, a new reference temperature T_r' having $f(T_r') = f'$ is calculated as $T_r' = T_r + \{f'-f(T_r)\}/\alpha_f$.

For bulk PI-20 and PtBS-16 systems, the WLF eqs 1 and 2 shown in the text give $f(T^{PI}_{r,bulk} = 30\ °C) = 0.098_1$ and $f(T^{PtBS}_{r,bulk} = 171\ °C) = 0.043_4$, respectively. Thus, we made the above WLF analysis for the a_T^{or} data of PI-20 (corrected for the restriction of DTD/CR due to PtBS-16) and the raw a_T data of PtBS-16 in the blends to find temperatures $T_{r,PI}'$ where $f(T_{r,PI}'$; in blend$) = 0.098_1$ and $T_{r,PtBS}'$ where $f(T_{r,PtBS}'$; in blend$) = 0.043_4$.

The motional unit for the global relaxation of polymers is the Rouse segment exhibiting the entropic elasticity. Since the local friction for this segment is considered to be determined by f, we utilized $T_{r,PI}'$ and $T_{r,PtBS}'$ explained above as the iso-frictional (iso-ζ) temperatures T_{iso} for PI-20 and PtBS-16 in the blends defined with respect to bulk PI-20 (at 30 °C) and PtBS-16 (at 171 °C), respectively. These T_{iso} data are summarized in Table 2. The shift factors $a_{T,iso}$ for PI-20 and PtBS-16 in the blends defined with respect to these T_{iso} were excellently described by the WLF equations for bulk PI-20 and PtBS-16 (cf. Figures 11 and 14), confirming that the T_{iso} values were satisfactorily obtained from the WLF analysis.

In relation to this result, a comment needs to be made for our choice of the *iso-ζ* temperature, T_{iso}. We can *formally* utilize the glass transition temperature T_g as the reference temperature T_r in eq B1 to describe the T dependence of a_T of our interest (the dependence at high T well above T_g). However, this dependence reflects the change of the local friction of the Rouse segment with T and is not directly related to the glass transition: The dynamic response of polymers in the glass transition zone is dominated by the relaxation of the *monomeric* segments, not of the Rouse segment.[22,37,38] Furthermore, the T dependence of a_T in the glass transition zone deviates from the WLF dependence[22] (partly because of this dominance by the monomeric segments) and the time−temperature superposition itself does not accurately holds in this zone.[37,38] For these reasons, the reference temperatures $T_{r,bulk}$ for bulk PI-20 and PtBS-16 were chosen to be well above T_g, $T_{r,bulk\text{-}PI} = 30$ °C (eq 1) and $T_{r,bulk\text{-}PtBS} = 171$ °C (eq 2) where the dominant part of the global relaxation was observed. Consequently, for the PI-20 and PtBS-16 chains in the blends, we chose the *iso-ζ* temperatures corresponding to these $T_{r,bulk}$'s.

References and Notes

(1) Lodge, T. P.; McLeish, T. C. B. *Macromolecules* **2000**, *33*, 5278–5284.
(2) Miller, J. B.; McGrath, K. J.; Roland, C. M.; Trask, C. A.; Garroway, A. N. *Macromolecules* **1990**, *23*, 4543–4547.
(3) Chung, G. C.; Kornfield, J. A.; Smith, S. D. *Macromolecules* **1994**, *27*, 964–973.
(4) Alegria, A.; Colmenero, J.; Ngai, K. L.; Roland, C. M. *Macromolecules* **1994**, *27*, 4486–4492.
(5) Kumar, S. K.; Colby, R. H.; Anastasiadis, S. H.; Fytas, G. *J. Chem. Phys.* **1996**, *105*, 3777–3788.
(6) Wetton, R. E.; Macknight, W. J.; Fried, J. R.; Karasz, F. E. *Macromolecules* **1978**, *11*, 158–165.
(7) Liang, K. M.; Banhegyi, G.; Karasz, F. E.; Macknight, W. J. *J. Polym. Sci., Part B: Polym. Phys.* **1991**, *29*, 649–657.
(8) Miura, N.; MacKnight, W. J.; Matsuoka, S.; Karasz, F. E. *Polymer* **2001**, *42*, 6129–6140.
(9) Pathak, J. A.; Colby, R. H.; Floudas, G.; Jerome, R. *Macromolecules* **1999**, *32*, 2553–2561.
(10) Pathak, J. A.; Colby, R. H.; Kamath, S. Y.; Kumar, S. K.; Stadler, R. *Macromolecules* **1998**, *31*, 8988–8997.
(11) Pathak, J. A.; Kumar, S. K.; Colby, R. H. *Macromolecules* **2004**, *37*, 6994–7000.
(12) Hirose, Y.; Urakawa, O.; Adachi, K. *Macromolecules* **2003**, *36*, 3699–3708.
(13) Hirose, Y.; Urakawa, O.; Adachi, K. *J. Polym. Sci., Part B: Polym. Phys.* **2004**, *42*, 4084–4094.
(14) Adachi, K. *Prog. Polym. Sci.* **1993**, *18*, 585–622.
(15) Watanabe, H. *Macromol. Rapid Commun.* **2001**, *22*, 127–175.
(16) Haley, J. C.; Lodge, T. P. *J. Rheol.* **2004**, *48*, 463–486.
(17) Haley, J. C.; Lodge, T. P.; He, Y. Y.; Ediger, M. D.; von Meerwall, E. D.; Mijovic, J. *Macromolecules* **2003**, *36*, 6142–6151.
(18) Watanabe, H.; Matsumiya, Y.; Takada, J.; Sasaki, H.; Matsushima, Y.; Kuriyama, A.; Inoue, T.; Ahn, K. H.; Yu, W.; Krishnamoorti, R. *Macromolecules* **2007**, *40*, 5389–5399.
(19) Yurekli, K.; Krishnamoorti, R. *J. Polym. Sci., Part B: Polym. Phys.* **2004**, *42*, 3204–3217.
(20) Takada, J.; Sasaki, H.; Matsushima, Y.; Kuriyama, A.; Matsumiya, Y.; Watanabe, H.; Ahn, K. H.; Yu, W. *Nihon Reoroji Gakkaishi (J. Soc. Rheol. Japan)* **2008**, *36*, 35–42.
(21) Fetters, L. J.; Lohse, D. J.; Colby, R. H., *Chain Dimensions and Entanglement Spacings, in Physical Properties of Polymers Handbook*, 2nd ed.; Mark, J. E., Ed.; Springer: New York, 2007; Chapter 25, pp 445−452.
(22) Ferry, J. D., *Viscoelastic Properties of Polymers*, 3rd ed.; Wiley: New York, 1980; Chapter 11, pp 264−320.
(23) Fetters, L. J.; Lohse, D. J.; Richter, D.; Witten, T. A.; Zirkel, A. *Macromolecules* **1994**, *27*, 4639–4647.
(24) Fetters, L. J.; Lohse, D. J.; Graessley, W. W. *J. Polym. Sci., Part B: Polym. Phys.* **1999**, *37*, 1023–1033.
(25) Extrapolating the χ data[19] for PI ($M_{PI} = 40._0 \times 10^3$) and PtBS ($M_{PtBS} = 33._3 \times 10^3$) reported as a function of T, we estimated, in the previous work,[18] the phase separation temperature of the PI-20/PtBS-70 blend as $T_c \cong 250$ °C.
(26) Graessley, W. W. *Adv. Polym. Sci.* **1974**, *16*, 1–179.
(27) Watanabe, H.; Matsumiya, Y.; Inoue, T. *Macromolecules* **2002**, *35*, 2339–2357.
(28) Watanabe, H. *Prog. Polym. Sci.* **1999**, *24*, 1253–1403.
(29) Pakula, T. *Dielectric and Mechanical Spectroscopy—a Comparison, in Broadband Dielectric Spectroscopy*; Kremer, F., Schönhals A., Eds.; Springer: Berlin, 2003; Chapter 16, pp 597−623.
(30) (a) Note that the coincidence of the dielectric and viscoelastic relaxation frequencies (within the factor of 2)[15,27,29] is a characteristic feature of the rubbery (global) relaxation of type-A polymers including PI. This coincidence is not found for the glassy (segmental) relaxation in polymeric/oligomeric materials[29,30b,c] because of several factors that possibly include a difference between the viscoelastically and dielectrically active segments. (b) McCrum, N. G.; Read, B. E.; Williams, G. *Anelastic and Dielectric Effects in Polymeric Solids*, Dover: New York, 1967, p. 300. (c) Buchenau, U. *J. Non-Cryst. Solids* **2007**, *353*, 3812–3819.
(31) The dielectric intensity of the global relaxation of PI chains, $\Delta\epsilon$, is proportional to $\nu R_{PI}^2/T$, where ν and R_{PI}^2 are the number density and mean-square end-to-end distance of the chain, respectively, and T is the absolute temperature.[14,15] Thus, strictly speaking, the intensity correction factor to be multiplied to the ϵ'' data at T is given by $\{T/T_r\}\{\nu R_{PI}^2\}_{Tr}/\{\nu R_{PI}^2\}_T$. However, changes of ν and R_{PI}^2 with T are much smaller than the change of T itself. For this reason, we can safely neglect the ν and R_{PI}^2 terms in the correction factor.
(32) (a) The global dielectric relaxation of PI chains detects the end-to-end vector fluctuation.[14,15] Thus, any heterogeneity over a length scale *much shorter* than the end-to-end distance is smeared in the global relaxation and can be just regarded as a factor determining a segmental friction averaged over the chain backbone. For this reason, the global dielectric mode distribution (being independent of this average friction) is insensitive to a change of the environment, unless the chains are subjected to strong thermodynamic/spatial confinements.[15] In contrast, the segmental relaxation detecting the dynamics at short length scales is very sensitive to changes in the environment;[32b,c] for example, the segmental mode distribution broadens on dilution with a solvent. (b)

Jones, A. A.; Inglefield, P. T.; Liu, Y.; Roy, A. K.; Cauley, B. J. *J. Non-Cryst. Solids* **1991**, *131*−*133*, 556–562. (c) Yada, M.; Nakazawa, M.; Urakawa, O.; Morishima, Y.; Adachi, K. *Macromolecules* **2000**, *33*, 3368–3374.
(33) Watanabe, H.; Ishida, S.; Matsumiya, Y.; Inoue, T. *Macromolecules* **2004**, *37*, 1937–1951.
(34) Angell, C. A. *J. Phys. Chem. Solids* **1988**, *49*, 863–871.
(35) Hodge, I. M. *J. Non-Cryst. Solids* **1996**, *202*, 164–172.
(36) Roland, C. M.; Ngai, K. L. *J. Non-Cryst. Solids* **1997**, *212*, 74–76.
(37) Inoue, T.; Okamoto, H.; Osaki, K. *Macromolecules* **1991**, *24*, 5670–5675.
(38) (a) Inoue, T.; Mizukami, Y.; Okamoto, H.; Matsui, H.; Watanabe, H.; Kanaya, T.; Osaki, K. *Macromolecules* **1996**, *29*, 6240–6245. (b) Inoue, T.; Uematsu, T.; Osaki, K. *Macromolecules* **2002**, *35*, 820–826.
(39) Ding, Y.; Sokolov, A. P. *Macromolecules* **2006**, *39*, 3322–3326.
(40) In the previous work,[20] we assumed that the PtBS-16 chains relaxing faster than PI-20 gave no constraint for the PI-20 motion in the blend with $w_{PtBS} = 20$ wt %. However, as judged from the result of comparison in the bottom panel of Figure 11, it is more reasonable to assume some constraint due to the PtBS-16 chains in this blend.
(41) Watanabe, H.; Sakamoto, T.; Kotaka, T. *Macromolecules* **1985**, *18*, 1008–1015.
(42) In the previous work[18] for PI-20/PtBS-70 blend with $w_{PtBS} = 20$ wt %, we neglected the contribution of the minority PI-20 to $G_{PI}^*(w,T)$ because the mode broadening due to the minority was just moderate and thus the minority content was small. However, for completeness, this contribution is incorporated in the analysis (eq 15) in this study.
(43) Mott, P. H.; Roland, C. M. *Macromolecules* **1998**, *31*, 7095–7098.
(44) Inoue, T.; Osaki, K. *Macromolecules* **1999**, *32*, 4725–4727.
(45) Roland, C. M.; Mott, P. H. *Macromolecules* **1999**, *32*, 4728–4728.
(46) Roland, C. M.; Archer, L. A.; Mott, P. H.; Sanchez-Reyes, J. *J. Rheol.* **2004**, *48*, 395–403.
(47) Inoue, T.; Matsui, H.; Murakami, S.; Kohjiya, S.; Osaki, K. *Polymer* **1997**, *38*, 1215–1220.
(48) Inoue, T.; Ryu, D. S.; Osaki, K. *Macromolecules* **1998**, *31*, 6977–6983.
(49) Doi, M.: Edwards, S. F. *The Theory of Polymer Dynamics*; Oxford University Press: New York, 1986; Chapter 7, pp. 218−288.
(50) (a) The Kuhn molecularw weight of PtBS, $M_{K,PtBS} \cong 1500$, was evaluated from the data for the characteristic ratio ($C_\infty = 13.0 \pm 0.7$)[50b] and a ratio of the mean-square end-to-end distance to molecular weight reported for PtBS,[21] $R_{PtBS}^2/M_{PtBS} = 0.0036_1$ (nm^2). (b) Mays, J. W.; Ferry, W. M.; Hadjichristidis, N.; Funk, W. G.; Fetters, L. J. *Polymer* **1986**, *27*, 129–132.
(51) Graessley, W. W. *Adv. Polym. Sci.* **1982**, *47*, 67–117.
(52) McLeish, T. C. B. *Adv. Phys.* **2002**, *51*, 1379–1527.
(53) Watanabe, H.; Ishida, S.; Matsumiya, Y.; Inoue, T. *Macromolecules* **2004**, *37*, 6619–6631.

MA8013417